Faculty of Engineering of University of Porto



Tumor-Targeting Engineered Nanoparticles for Antioxidant Therapy

Bruna da Silva Alves

Master dissertation
Master's in Biomedical Engineering

Supervisor: Prof. Dr. Maria do Carmo Pereira
Co-Supervisor: Dr. Maria João Ramalho

Porto, June 2023

© Bruna da Silva Alves, 2023

Financial Support

This work was financially supported by: LA/P/0045/2020 (ALiCE), UIDB/00511/2020 and UIDP/00511/2020 (LEPABE), funded by national funds through FCT/MCTES (PIDDAC), funded by FEDER funds through COMPETE2020 – Programa Operacional Competitividade e Internacionalização (POCI) and by national funds (PIDDAC) through FCT/MCTES; Project 2SMART - engineered Smart materials for Smart citizens, with reference NORTE-01-0145-FEDER-000054, supported by Norte Portugal Regional Operational Program (NORTE 2020), under the PORTUGAL 2020 Partnership Agreement, through the European Regional Development Fund (ERDF). This project has received funding from the European Union's Horizon 2020 research and innovation program under grant agreement No 958174; and from national funds through FCT (M-ERA-NET3/0001/2021).







Resumo

O glioblastoma multiforme (GBM) é um tumor maligno que afeta o sistema nervoso central (SNC). O seu tratamento convencional passa por cirurgia, seguido de radioterapia e quimioterapia. No entanto, a barreira hematoencefálica (BHE) que impossibilita a passagem da maioria dos agentes terapêuticos até ao tumor é uma das principais limitações da terapia. A encapsulação de fármacos em nanopartículas (NPs) é uma alternativa de forma a conseguir ultrapassar a BHE e atingir o tecido alvo com sucesso.

Neste sentido, o objetivo deste trabalho foi desenvolver NPs de poli(ácido lático-co-glicólico) (PLGA) para a encapsulação do composto natural ácido gálico (AG) devido às suas propriedades antioxidantes e anticancerígenas. As NPs foram modificadas com ácido fólico (AF), dado a sobreexpressão do seu recetor nas células tumorais, contribuindo para o direcionamento ativo das NPs.

A preparação das NPs foi optimizada utilizando o modelo Design Composto Central (DCC). As NPs obtidas têm propriedades físico-químicas adequadas para internalização do fármaco no tecido tumoral, apresentando uma eficiência de encapsulação (EE) de 50% e perfil de libertação controlado em condições fisiológicas ao longo de 15 dias. Ensaios celulares *in vitro* nas linhas celulares U251 e NHA revelaram que a terapia com GA livre inibiu a proliferação celular mais eficientemente do que a terapia com NPs, o que pode ser explicado devido à lenta libertação do GA. Adicionalmente, foi possível concluir que as NPs são biocompatíveis.

Palavras-chave: Glioblastoma multiforme; Barreira Hematoencefálica; Nanopartículas; Poli (ácido lático-co-glicólico); Ácido Gálico; Ácido Fólico; Desenho experimental; Eficiência de Encapsulação.

Abstract

Glioblastoma multiforme (GBM) is a malignant tumor that affects the central nervous system (CNS). Its conventional treatment involves surgery, followed by radiation therapy and chemotherapy. However, the blood-brain barrier (BBB) that makes it impossible for most therapeutic agents to pass through to the tumor is one of the main limitations of therapy. The encapsulation of drugs in nanoparticles (NPs) is an alternative to overcome the BBB and successfully reach the target tissue.

In this sense, the aim of this work was to develop poly(lactic-co-glycolic acid) (PLGA) NPs for the encapsulation of the natural compound gallic acid (GA) due to its antioxidant and anticancer properties. The NPs were modified with folic acid (FA), given the overexpression of its receptor in tumor cells, contributing to the active targeting of the NPs.

The preparation of the NPs was optimized using the Central Composite Design (CCD) model. The obtained NPs have physicochemical properties suitable for drug internalization in tumor tissue, showing an encapsulation efficiency (EE) of 50% and a controlled release profile under physiological conditions over 15 days. *In vitro* cell assays on U251 and NHA cell lines revealed that free GA therapy inhibited cell proliferation more efficiently than therapy with NPs, which can be explained due to the slow release of GA. Additionally, it could be concluded that NPs are biocompatible.

Keywords: Glioblastoma multiforme; Blood-brain Barrier; Nanoparticles; Poly (lactic-co-glycolic acid); Gallic Acid; Folic Acid; Central Composite Design; Encapsulation Efficiency.

Acknowledgments

With the culmination of my academic journey, it is important to express my deepest gratitude and appreciation to all those who supported and guided me throughout it.

Firstly, I would like to thank my supervisors Prof. Dr. Maria do Carmo Pereira and Dr. Maria João Ramalho for their guidance, help, experience, and knowledge transmission that were fundamental to shaping this thesis and improving my research skills. I thank Dr. Paula Soares and Dr. Jorge Lima from the Cancer Signaling and Metabolism Group of the Institute for Research and Innovation in Health Sciences (i3S) for providing the facilities to perform the cellular studies. I would also like to thank my laboratory colleagues at LEPABE and DEQ, who supported and assisted me along this path.

I would also like to express my gratitude to my friends for their friendship, motivation, and words of encouragement.

In addition, I am deeply grateful to my family for their unwavering support, love, and encouragement. Their belief in my abilities and encouragement were undoubtedly unconditional.

I am truly grateful to all those mentioned above, as well as others who supported me in various ways during this research work. Thank you very much.

Contents

Financial Support ..... **iii**

Resumo ..... **v**

Abstract ..... **vii**

Acknowledgments ..... **ix**

Contents ..... **xi**

List of Figures ..... **xiii**

List of Tables ..... **xv**

Abbreviations, Acronyms and Symbols ..... **xvi**

Chapter 1 ..... **19**

Introduction 19
1.1 Structure of the Dissertation 19
1.2 Dissertation Output 20

Chapter 2 ..... **21**

State of the Art 21
2.1 Glioblastoma Multiforme 21
2.2 Conventional Treatment of GBM and its Limitations 22
2.3 Natural Compounds for the Treatment of GBM 23
2.3.1 Role of Gallic Acid in GBM Treatment 24
2.4 Brain Delivery of Natural Compounds for GBM 26
2.4.1 Nanomedicine 27
2.4.2 Overcoming the blood-brain barrier 29
2.4.3 Currently Developed NPs for Natural Compounds Brain Delivery in GBM 31

Chapter 3 ..... **40**

Materials and Methods 40
3.1 Materials 40
3.2 Preparation of the Gallic Acid-loaded PLGA NPs 41
3.3 Functionalization of GA-PLGA NPs with Folic Acid 41
3.4 Experimental Design and Protocol Optimization 42
3.5 NPs Physicochemical Characterization 44
3.5.1 Dynamic Light Scattering 44
3.5.2 Laser Doppler Velocimetry 45
3.6 Determination of Encapsulation Efficiency 46
3.7 Fourier-Transformed Infrared Spectroscopy 47
3.8 Transmission electron microscopy (TEM) 47
3.9 *in vitro* Release Experiments 48
3.10 Evaluation of NPs' Stability 48
3.11 Cell Culture 49
3.12 Sulforhodamine B assay 49
3.13 Statistical Analysis 50

Chapter 4 51

Results and Discussion 51
4.1 Experimental Design and Protocol Optimization 51
4.1.1. Effect on the NPs' Size 55
4.1.2. Effect on NPs' PDI 56
4.1.3. Effect on NPs' Zeta Potential 58
4.1.4. Effect on GA EE 59
4.2 Protocol Optimization and Model Validation 60
4.3 FTIR Analysis 61
4.4 TEM Analysis 63
4.5 Release Profile of GA 63
4.6 NPs' Stability in Storage Conditions 64
4.7 NPs' Stability in Physiological Conditions 65
4.8 NPs' Antiproliferative Activity 66

Chapter 5 69

Conclusions and Future Perspectives 69

References 71

Appendix 84

A1. Calibration Curve 84

A2. Experimental Design 85

A3. GA Solubility and Stability Studies 89

List of Figures

Figure 1 - Chemical structure of GA. 25

Figure 2 - Comparison between normal and dysfunctional lymphatic systems [56]. 27

Figure 3 - Types of NPs in nanomedicine.....29

Figure 4 - Chemical reactions between FA and polymeric NPs catalyzed by EDC. 41

Figure 5 - Representation of the electric double layer. 46

Figure 6 - Graphical plots between the experimental values obtained vs the predicted values for the significant variables, (A) Size (Y_1), (B) PDI (Y_2), (C) Zeta Potential (Y_3), and (D) GA EE (Y_4). The blue squares represent lower values, in contrast to red squares that represent higher values. 53

Figure 7 - (A)(B) Contour and (C)(D) surface plots of all independent variables on the NPs' size. 55

Figure 8 - (I)(III) Contour and (II)(IV) surface plots of all independent variables on the NPs' PDI.....57

Figure 9 - (A)(C) Contour and (B)(D) surface plots of all independent variables on the NPs' Zeta Potential. 58

Figure 10 - (A) Contour and (B) surface plots of PLGA mass and % of PVA on the NPs' EE of GA. 59

Figure 11 - FTIR absorbance spectra of (A) GA-PLGA NPs and (B) Stock FA. 62

Figure 12 - FTIR absorbance spectrum of FA-GA-PLGA NPs, PLGA NPs, and FA stock solution. 62

Figure 13 - Morphological characterization of FA-GA-loaded PLGA NPs by TEM. 63

Figure 14 - Release profile of FA-GA-loaded PLGA NPs overtime for pH=7.4 and 6.4. 64

Figure 15 - Cell survival curve after 72-hour treatment with free GA and FA-GA-NPs for (A) NHA cell line (B) U251 cell line. 67

Figure 16 - Cell survival rate of FA-PLGA NPs for U251 and NHA cell lines. 68

Figure A1. 1- Absorbance calibration curve of GA in PVA 1% to determine the EE of GA. 84

Figure A3. 1- Solubility of GA in ethyl acetate. .....**Error! Bookmark not defined.**

Figure A3. 2- Solubility of GA in DMSO. .....**Error! Bookmark not defined.**

Figure A3. 3- Stability of GA in ethyl acetate. 91

List of Tables

Table 1- Examples of current clinically approved nanoformulations on the market [57]. 28

Table 2- Natural Compounds for GBM Therapy. 31

Table 3- Independent variables and varying levels used in the experimental design. 42

Table 4- Experimental design and obtained responses of all 30 nanoformulations. The experimental levels (low, center, high, and alpha) are represented by -1, 0, +1, and α, respectively. 43

Table 5- Results of the statistical analysis using ANOVA. 52

Table 6 – RC and p-Value for all responses. 54

Table 7- Optimal formulation prediction for GA loaded PLGA NPs. 60

Table 8- Predicted *versus* experimental values. The experimental results are represented as mean ± SD (n=5) 60

Table 9- Optimal FA-GA-loaded PLGA NPs stability in storage conditions over 6 weeks (mean±SD, n=5). 64

Table 10- Optimal FA-GA-loaded PLGA NPs stability in physiological conditions over 2 weeks. 65

Table 11 - IC_{50} after 72 hours using free GA and FA-GA-NPs for both cell lines. 67

Table A2. 1 - ANOVA analysis for the response variable Size (Y_1) applying a quartic model. 85

Table A2. 2 - ANOVA analysis for the response variable PDI (Y_2) applying a quartic model. ...86

Table A2. 3 - ANOVA analysis for the response variable Zeta Potential (Y_3) applying a quartic model. 87

Table A2. 4 - ANOVA analysis for the response variable GA EE (Y_4) applying a linear model. ..88

Abbreviations, Acronyms and Symbols

Lists of abbreviations

AA	Asiatic Acid
ANOVA	Analysis of Variance
ATR	Attenuated Total Reflectance
BA	Betulinic Acid
BBB	Blood-Brain Barrier
BBD	Box-Behnken Design
BBTB	Brain-Blood Tumor Barrier
CCD	Central Composite Design
CTX	Cabazitaxel
CNS	Central Nervous System
CPT	Camptothecin
CUR	Curcumin
DDS	Drug Delivery System
DLS	Dynamic Light Scattering
DMEM	Dulbecco's Modified Eaglec Medium
DMSO	Dimethyl Sulfoxide
DoE	Design of Experiment
EA	Ethyl Acetate
EDC	1-ethyl-3-(3-dimethylaminopropyl) carbodiimide
EE	Encapsulation Efficiency
EGFR	Epidermal Growth Factor Receptor
EPR	Enhanced Permeability and Retention
EMA	European Medicines Agency
FA	Folic Acid

FBS	Fetal Bovine Serum
FDA	Food and Drug Administration
FTIR	Fourier-Transformed Infrared Spectroscopy
GA	Gallic Acid
GBM	Glioblastoma Multiforme
Gen	Genistein
IC_{50}	Half Maximal Inhibitory Concentration
IDH	Isocitrate Dehydrogenase
KPF	Kaempferol
MGMT	O6-Methylguanine-DNA methyltransferase
MLT	Melatonin
MRI	Magnetic Resonance Imaging
MW	Molecular Weight
NE	Nanoemulsions
NF1	Neurofibromin 1
NHA	Normal Human Astrocytes
NPs	Nanoparticles
NNI	National Nanotechnology Initiative
OFAT	One Factor at a Time
PBS	Phosphate Buffered Saline
PCL	Poly (caprolactone)
PDGFRA	Platelet-derived Growth Factor Receptor Alpha
PDI	Polydispersity Index
PLGA	Poly (lactic-co-glycolic acid)
PMMs	Polymeric Mixed Micelles
PTEN	Phosphatase and Tensin Homolog
PVA	Polyvinyl Alcohol
Qu	Quercetin
RES	Resveratrol
Rpm	Rotations per minute
SD	Standard Deviation
SRB	Sulforhodamine
TCA	Trichloroacetic Acid
TCGA	The Cancer Genome Atlas Research
TEM	Transmission Electron Microscopy
Tf	Transferrin
Tfr	Transferrin receptors
TJs	Tight Junctions
TMZ	Temozolomide

UV	Ultra-violet
VS	Vascular System
WHO	World Health Organization

Lists of symbols

A	Alpha
μ_e	Electrophoretic mobility
ε_r	Dielectric constant
η	Viscosity
ζ	Zeta potential
v	Velocity
E	Electric field
k	Boltzmann constant
T	Absolute temperature
D	Translation diffusion coefficient
R_H	Hydrodynamic radius

Chapter 1

Introduction

Glioblastoma multiforme (GBM) is part of the family of malignant gliomas, being highly proliferative, aggressive, and invasive. Thus, this type of cancer has a reduced survival rate, with a high probability of recurrence. The treatment of this disease involves surgical resection, followed by chemotherapy and radiotherapy, which can prolong the survival time of young patients by up to 202 weeks [1].

In addition, the anatomical location of this malignant tumor implies the passage of the therapeutic agent through the blood-brain barrier (BBB), which is quite difficult since this physiological barrier does not allow the passage of most compounds through it. In this sense, it is important to develop therapies that allow better performance in the treatment of this disease, such as the use of nanoparticles (NPs) for drug delivery [2].

Gallic Acid (GA) is a natural phenolic compound, present in various fruits and herbs, which can be applied in drugs to fight cancer, microbial infections, and cardiovascular diseases due to its antioxidant and anti-cancer properties [3]. However, their therapeutic effects often cannot be achieved due to rapid metabolism and low bioavailability. One solution is to use nanoformulations for encapsulation of this drug to enhance these properties and thus improve drug delivery in tumor tissue [4].

This project aims to develop nanoparticles (NPs), using the emulsion-simple method, for the encapsulation of natural compounds, namely gallic acid (GA), in the treatment of GBM. To improve their performance, the NPs were functionalized with folic acid (FA), since this compound has an overexpression of receptors in tumor cells, which will increase the specificity and therapeutic efficacy [5].

1.1 Structure of the Dissertation

This dissertation is organized into five distinct chapters. Chapter 1 introduces the subject of the work and its main objectives. Chapter 2 represents the state of the art, where the main topics and concepts are addressed, namely the approach to GBM disease, its standard treatment, and the limitations associated with it, as well as the use of natural compounds in nanomedicine as new approaches to the treatment of this disease. Chapter 3 presents the methodologies used in the realization of this project. Chapter 4 focuses on the presentation and discussion of the results obtained, culminating in Chapter 5, where the main conclusions of the work and future perspectives are presented.

1.2 Dissertation Output

The research work was carried out at LEPABE – Laboratory for Process Engineering Environment, Biotechnology, and Energy at the Faculty of Engineering of the University of Porto. The *in vitro* studies were performed at i3S – Institute for Research and Innovation in Health.

This work was presented at a conference:

Alves, Bruna, Loureiro, Joana. A., Ramalho, Maria João and Pereira, Maria Carmo. *Tumor-targeting nanoparticles for glioblastoma therapy with antioxidant compounds*. in 16th Encontro de Investigação Jovem da Universidade do Porto (IJUP), 10-12 May 2023, Porto, Portugal (*oral presentation)*.

Chapter 2

State of the Art

2.1 Glioblastoma Multiforme

Glioblastoma Multiforme (GBM) are malignant tumors of the central nervous system (CNS) [6]. This type of tumor is a subtype of primary brain tumors, called gliomas, which can be classified into astrocytic tumors, oligodendrogliomas, ependymomas, and mixed gliomas, depending on their cell origin. According to their level of malignancy, gliomas are classified into four grades (I to IV), established by the World Health Organization (WHO) [7]. In this way, GBM is a grade IV primary astrocytoma due to its aggressiveness and invasiveness [8].

This malignant tumor can be divided into primary or secondary GBMs regarding its clinical form: primary GBMs are the most common, accounting for approximately 90% of the cases, and occur mostly *de novo* in older patients, without clinical antecedents; on the opposite, secondary GBMs are more prevalent in younger patients, exhibiting a slower progression (10-15 years) and are derived from prior low-grade astrocytoma [9], [10]. Besides that, in secondary GBM the level of tissue necrosis is lower, and the tumor is usually located in the frontal lobe. The prognosis for secondary GBM is considerably better when compared with the primary type [9]. There are also some molecular differences between both, for example, in primary GBMs, the epidermal growth factor receptor (EGFR) is mutated and amplified, and in secondary form, there is increased signaling in platelet-derived growth factor receptor alpha (PDGFRA) [8]. Despite the complexity and heterogeneity of gene expression presented by GBM, some molecular markers have been identified, due essentially to their overexpression and amplification, as examples are EGFR, isocitrate dehydrogenase (IDH-1/2), and O6-methylguanine-DNA methyltransferase (MGMT) [10], [11].

According to The Cancer Genome Atlas Research (TCGA), GBMs can also be classified into four transcriptional subclasses based on their genetic and epigenetic markers [10]. These subtypes are classical, mesenchymal, proneural, and neural, which represent different expression profiles and genetic alterations [12]. The mesenchymal subtype is characterized by neurofibromin 1 (NF1) tumor suppressor gene mutation and frequent mutations in some tumor suppressor genes like phosphatase and tensin homolog (PTEN) and TP53. The classical subtype doesn't have TP53 mutation but presents amplification in EGFR and is extremely proliferative. These two types are the most aggressive tumors. The proneural GBM is characterized by mutations in IDH1, PDGFRA, and TP53. The last subtype, neural, has many genes that are also characteristics of noncancerous neurons [13].

Even though the global incidence is 2 to 5 cases per 100,000 people, these tumors represent more than 49% of all primary malignant brain tumors, with a median survival rate of 14 to 15 months after diagnosis [14]–[16]. Is estimated that each year, 250,000 new cases of GBM appear worldwide [15]. This cancer has a 6.8% of five-year survival rate and a mean age of 64 years for a diagnosis [16]. The incidence of GBM has grown in the past 20 years, probably as a result of the improvement in medicine, specifically in radiologic diagnosis [17]. Additionally, the prevalence of these tumors increases with age, being higher in men than women (1.5 times more) and Caucasians when compared with other ethnic groups (2 times more) [18].

Beyond being life-threatening, this tumor also has a negative effect on patients' daily basis as a consequence of brain damage, resulting in the loss of their cognition, behavior, and body control [16]. Clinically, patients who have been diagnosed with GBM can reveal symptoms like headaches, focal neurologic deficits, confusion, memory loss, and personality changes [19].

GBM is characterized by variations in tumor appearance from one brain region to another, showing heterogeneity. These types of tumors show a wide range of cell differentiation, ranging from poorly differentiated tumor cells to multinucleated cells with necrosis [20].

2.2 Conventional Treatment of GBM and its Limitations

Although there are currently numerous efforts to improve the therapy of these tumors, the treatment of GBM is still a clinical challenge due to its heterogeneity, complexity, location, and acquired resistance to chemotherapy, making their treatment even more challenging [21].

The conventional approach for GBM diagnosis is magnetic resonance imaging (MRI) since it has high anatomical resolution and great soft tissue contrast [22]. The GBM gold standard treatment is essentially based on surgical resection of the tumor followed by radiotherapy cycles combined with chemotherapy [23]. The purpose of surgery is to remove as much of the tumor mass as possible and also to define the histopathological diagnosis of the tumor. From this analysis, it is possible to determine which therapy will best increase the patient's survival rate [11].

Since GBM is a very invasive tumor, it is not possible to totally remove it at surgery, is necessary to follow it with radiotherapy and adjuvant temozolomide (TMZ), to kill the tumor cells that are still present in the brain [24]. Thus, during the first 6 weeks, radiotherapy is performed in 2 gray fractions (Gy) for a total dose of 40-60 Gy in conjunction with TMZ 75 mg/m^2 followed by 6 months (6 cycles) of adjuvant TMZ 150-200 mg/m^2 every 28 days [25].

However, some limitations and risk factors are associated with radiotherapies such as radiation necrosis, radiation-induced permanent neuronal damage, and radio-resistance of some tumors [26]. Intensity-modulated radiation therapy and boron neuron capture therapy are newer radiation therapies with lower toxicity to healthy tissues and have the same efficacy as conventional radiotherapy. These newest types of radiation are being used in patients with malignant gliomas to test their efficacy [27], [28].

It should also be noted that the recurrence of this type of tumor is high, with most patients presenting tumor recurrence within 6.9 months after diagnosis. When this occurs, reoperation or re-irradiation is often not allowed, and the best treatment option for these patients is clinical trials [29].

Simultaneously with radiation therapy, chemotherapy is performed usually with TMZ. This is an alkylating agent, used for standard chemotherapy since 1999. It has optimal penetration into the CNS and its bioavailability is around 96-100%. It is responsible for promoting the methylation of the O6 position in guanine (N7-guanine and N3 adenine). Its use has slightly increased the survival rate of GBM patients, however, there are side effects such as nausea and myelosuppression that compromise its use [30].

Besides TMZ, other alkylating drugs such as nitrosoureas, carmustine (1,2 bis[2-chloreoethyl]-1-nitrosourea BCNU), and lomustine (CCNU) are used in the treatment of GBM. These drugs are also associated with side effects such as nausea, vomiting, skin rashes, and pulmonary fibrosis. BCNU is the second most widely used agent for GBM therapy after TMZ. Despite its approval, the administration is not widely used due to slow healing, intracranial edema, cerebrospinal fluid leak, and intracranial infection [31].

Thus, to obtain better results, it is necessary to overcome some challenges that continue to prevent effective treatment of GBM, among which: incomplete tumor resection, high degree of genetic heterogeneity, unique blood-brain barrier (BBB), immunosuppressive microenvironment and high toxicity of the therapies [18].

2.3 Natural Compounds for the Treatment of GBM

Natural compounds are substances with therapeutic potential due to their well-known biological benefits [26], [32]. For this reason, natural products have been found in various medical applications since the beginning of medicine and are still present today [33]. Thus, in

recent years, several studies have emerged to investigate the influence of these types of compounds in fighting cancer, particularly its development and progression [34].

Currently, there is a wide range of natural substances that are recognized for their antioxidant, anti-inflammatory properties, and cancer chemopreventive potential [34]. Several studies have shown that using natural compounds to fight different types of cancer may be a way forward due to their effectiveness [33]. Between 1980 and 2019, the percentage of new drugs derived from natural products in combating cancer was approximately 25% [26].

Regarding GBM, there are several natural substances, such as curcumin, cardamom, and resveratrol, among others, that exhibit oncological effects *in vitro* and *in vivo*. Park et al. (2019) studied the effects of curcumin on anti-migration and anti-invasion in GBM cells. The results showed that curcumin suppresses the expression of fascin (the actin-binding protein that is related to the migration and invasion of GBM cells), thus revealing its oncological effect [35]. Manjunath and Mahurkar (2019) evaluated the cytotoxicity of cardamom, *in vitro*, using brain cancer cell lines. The results obtained showed that cardamom is one of the compounds with above-average antitumor activity [36]. Zou et al. (2017) investigate the neuroprotective effect of resveratrol against tumor brain injury, *in vivo*. The results showed that this compound is able to reduce tumors [37]. When compared to synthetic drugs used to treat cancer, natural compounds have greater efficacy and less toxicity to the body. Although this wide range of compounds exhibits anti-glioma activity, their eligibility for clinical approval is still scarce [33]. Thus, despite the high variety of natural compounds with anti-cancer properties for GBM, it is necessary to proceed and have the validation of clinical trials to corroborate their efficacy and demonstrate safety in their use, which so far is still a challenge to overcome [32].

2.3.1 Role of Gallic Acid in GBM Treatment

Gallic acid (GA), 3,4,5-trihydroxy benzoic acid, is a natural polyhydroxyphenolic compound that is found in various foods and plants such as nuts, hazelnuts, cloves, tea leaves, strawberries, and others [38], [39]. This compound has a yellowish-white color and a melting point of 250°C. Its molecular weight is 170.12 Da and it has a solubility of water at 20°C of 11.0 µg/mL [40]. In addition, GA is soluble in alcohol, ether, glycerol, and acetone [41]. Figure 1 represents the chemical structure of GA.

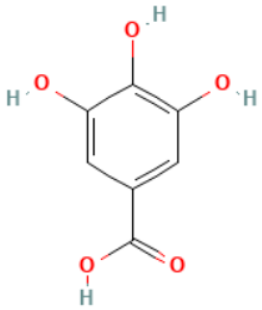


Figure 1 - Chemical structure of GA.

This compound is usually obtained from its precipitation from an aqueous solution with concentrated sulfuric acid. GA can also be produced by acid hydrolysis of tannic acid, microbial hydrolysis of tannic acid by tannase, or released by the oxidation of gallotannins [41].

GA exhibits several biological properties: anti-bacterial, anti-viral, antioxidant, and anti-carcinogenic [42]. Due to these characteristics, it is widely applied in several fields of science and medicine, namely in the treatment of arthritis and fungal infections [39]. In addition, several foods containing this substance have been used as natural remedies for many years. Derivatives of this substance are also widely used and researched by science that, due to their biological properties, can also have positive effects against different types of diseases [41].

The anti-carcinogenic activity of GA has already been shown in several *in vitro* and *in vivo* studies for different types of cancer: lung, prostate, breast, leukemia, GBM, and others [43]. GA is characterized by having low toxicity, which induces cancer cell death without damaging normal cells [39], [40]. Also, GA has a low price.

According to Yong et al., GA can suppress proliferation, metastasis, and angiogenesis in human glioma cells (U87 and U251) through a disintegrin and metalloprotease 17 (ADAM17) suppression and down-regulation of PI3K/Akt and Ras/MAPK signaling pathways. Through mitochondrial apoptotic pathways, it was shown that this compound also induces cell death of other human GBM cells (DBTRG-05MG) and does not compromise the viability of healthy cells, namely astrocytes, in mouse brain endothelial cells, *in vitro*. It was also verified through other studies that GA can decrease AKT and MAPK pathways, inhibiting cell proliferation and growth of U87 and T98G cells [44].

Although several studies have been developed over the past decades for the treatment of different types of cancer, namely lung cancer, prostate cancer, and stomach cancer, using GA, more clinical trials are needed to improve the therapeutic potential of GA for GBM therapy [39]. Even though GA has been reported to exhibit cytotoxicity for GBM cell lines, its effect on cells exposed to radiation is not yet clearly known [43]. Also, its bioavailability has been evaluated in different animal models [41]. This natural compound, when used in the body in free form shows rapid absorption but its concentration on the target tissue is low. In addition,

it should also be noted that it is relatively easily eliminated from the body, thus presenting a rapid metabolism [42].

Furthermore, achieving an improvement in the distribution of GA in the brain area will allow this compound to be more effective [42]. Thus, the advancement in the research of GA may be a roadmap for its clinical applicability to be an achievable goal in the near future [40]. Thus, different studies suggest that its use be carried out in conjunction with innovative technologies, such as nanodelivery so that its properties can be improved and greater effectiveness and efficiency in its use can be achieved.

2.4 Brain Delivery of Natural Compounds for GBM

Natural compounds have shown great potential for the treatment of different brain malignancies such as GBM. However, their systemic administration has several limitations. Most natural compounds have low solubility and stability which decreases their bioavailability in the target tissues, compromising their use [45].

Additionally, the BBB poses a major obstacle to brain delivery. The BBB separates the vascular system from the CNS and is extremely important in regulating brain homeostasis [46]. The BBB consists mainly of specialized endothelial cells connected by tight junctions (TJs) [47]. The endothelial cells form a thin layer, and it is through the TJs that they connect and exert their barrier properties by interacting with astrocytes, pericytes, and perivascular macrophages, thus forming the neurovascular unit. In addition, they also exhibit reduced pinocytotic activity and prevent paracellular transport [48].

The BBB conducts the regulation of the influx and efflux of ions, macromolecules, and nutrients to and from the brain. Thus, it protects the brain, preventing its direct exposure to pathogens and potentially harmful agents, and ensures brain nutrition, allowing the brain to function properly by isolating the brain tissue from the blood vascular system[49]. Approximately 98% of small molecules and 100% of macromolecules are prevented from crossing the BBB due to the presence of TJs, with only 2% of small molecules such as anxiolytics, antipsychotics, and opioids crossing this barrier [47], [50]. Thus, only a few molecules, with specific properties such as small lipophilic molecules with molecular weight (MW) less than 400-500 Dalton (Da) and less than nine hydrogen bonds, can diffuse through the BBB by simple diffusion [46]. In addition, the efficiency of this process also depends on the lipid solubility and the electrical charge of the solutes [49]. Other substances, such as nutrients, use transporters located in the membranes to overcome this barrier.

Most molecules need a transport system that allows them to cross this barrier since many of them are not absorbed by it [34]. The permeability of the BBB is a key factor in therapeutic efficacy, which varies greatly between different compounds. Thus, it becomes paramount that drugs cross the BBB to be effective in treating brain diseases such as GBM. It is also important

to mention that the high bioavailability of a natural compound but low permeability in the BBB, or vice versa, is insufficient since both factors are crucial for the drug to reach the tumor cells and minimize the toxicity towards the healthy cells [32].

2.4.1 Nanomedicine

Nanotechnology is a multidisciplinary field that has had, in recent decades, extreme importance and applicability in various areas, particularly in the industrial and medical fields. This technology is defined according to the National Nanotechnology Initiative (NNI) as "a science, engineering, and technology conducted at the nanometer scale (1 to 100 nm), where unique phenomena allow novel applications in a wide range of fields, from chemistry, physics, and biology, to medicine, engineering, and electronics." [51]. Thus, nanotechnology involves the design, production, characterization, and application within the nanoscale dimension [52].

Therefore, nanomedicine arises, which represents the application of nanotechnology in health, and may thus revolutionize the diagnosis and treatment of certain diseases, particularly cancer, since it can offer solutions to overcome the current limitations of clinical treatment such as chemotherapy and radiotherapy. Drug encapsulation into nanoparticles (NPs) allows to increase their stability and effectively deliver them to the target tissues with reduced side effects. NPs are advantageous for cancer therapy since they can infiltrate the tumor tissue with high specificity and make significant progress in their treatment [53]. Tumors usually have a poorly draining lymphatic vasculature, which is subsequently reflected in abnormal permeabilization of the vascular system. This phenomenon is known as the enhanced permeability and retention (EPR) effect. This effect allows NPs to accumulate within the tumor tissue, followed by the release of therapeutic substances [54]. This approach implies, however, that the transport of NPs takes place for particles with a size between 7-200 nm since the existing vascular ranges are in this scope [55]. Figure 2 represents the difference between the normal lymphatic system and the dysfunctional lymphatic system.

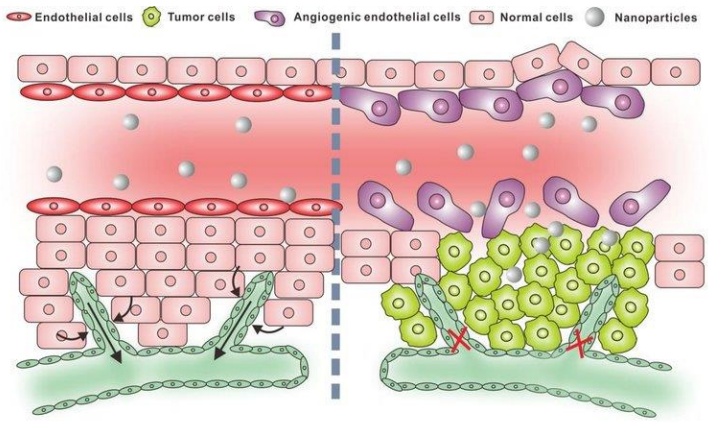


Figure 2 - Comparison between normal and dysfunctional lymphatic systems [56].

Currently, there are drug delivery systems (DDS) for anti-cancer drugs in clinical use, representing the great potential of this area. According to Anselmo and Mitragotri (2019), by 2016, more than 25 nanomedicines had been approved by Food and Drug Administration (FDA) or European Medicines Agency (EMA). In 2019, three new nanomedicines joined this list (Patisiran/ONPATTRO, VYXEOS, and NBTXR3/Hensify) and more than 15 new NP-based technologies started clinical trials [57]. Table 1 presents some of the nanoformulations that are recurrently on the market.

Table 1 - Examples of current clinically approved nanoformulations on the market [57].

Name (company)	Particle type/drug	Approved application/indication	Approval (year)
Onivyde MM-398 (Merrimack)	Liposomal irinotecan (PEGylated)	Metastatic pancreatic cancer (secondary)	FDA (2015)
NBTXR3 Hensify (Nanobiotix)	Hafnium oxide nanoparticles stimulated with external radiation to enhance tumor cell death via electron production	Locally advanced squamous cell carcinoma	CE Mark (2019)
Myocet (Teva UK)	Liposomal doxorubicin (non-PEGylated)	Treatment of metastatic breast cancer (primary)	EMA (2000)
VYXEOS CPX-351 (Jazz Pharmaceuticals)	Liposomal formulation of cytarabine: daunorubicin (5:1M ratio)	Acute myeloid leukemia	FDA (2017) EMA (2018)

Besides cancer therapy, nanomedicine has been widely explored for drug delivery of pharmaceuticals for the treatment of other diseases; diagnostics; regenerative medicine, and implantable devices [58]. This approach enables to allow using drugs or materials used, which were often compromised due to the reduced solubility, bioavailability, or rapid metabolism of the substance [45].

In this way, the idea behind this technology seeks to design nanoscale materials and devices with unique therapeutic properties, such as optical, electronic, or structural features, that are often not available in the materials in question through their bulk solids/individual molecules [59].

There are several ways to classify NPs, one of which is to divide them into two distinct groups, considering their chemical components: organic NPs and inorganic NPs. Within organic NPs, there are liposomes and polymeric NPs. The firsts are characterized by spherical vesicles composed of phospholipids. These vesicles can fuse with the cell membrane to selectively

deliver their contents and therefore are widely used for drug delivery to fight cancer. Polymeric NPs can be synthetic (poly (lactic-co-glycolic acid) (PLGA)) or natural (chitosan), with great biodegradability, biocompatibility, and non-toxicity, being the most used NPs in the drug delivery systems industry [60], [61].

Regarding inorganic NPs, these can be divided into: metallic NPS, which include precious metals (gold or silver), and magnetic metals (iron oxide or cobalt)[60]. In addition to being stable, easily synthesized, and biocompatible, magnetic NPs have magnetic properties [61]; metal oxide NPs, which are essentially composed of iron oxide (Fe_3O_4), titania (TiO_2), or zirconia (ZrO_2), with high chemical stability, optical properties, and biocompatibility [60]; ceramic NPs: normally composed of silica or aluminum but may also be composed of combinations of metallic and non-metallic materials, which can transport molecules or drugs; quantum dots: NPs composed of semiconductor or nanocrystal materials and present fluorescent properties. They are usually coated with a shell, such as zinc sulfide (ZnS), to optimize their properties, however, their use in the medical field is not yet consensual [60], [61]. Figure 3 schematically represents the different types of NPs that can be found in nanomedicine.

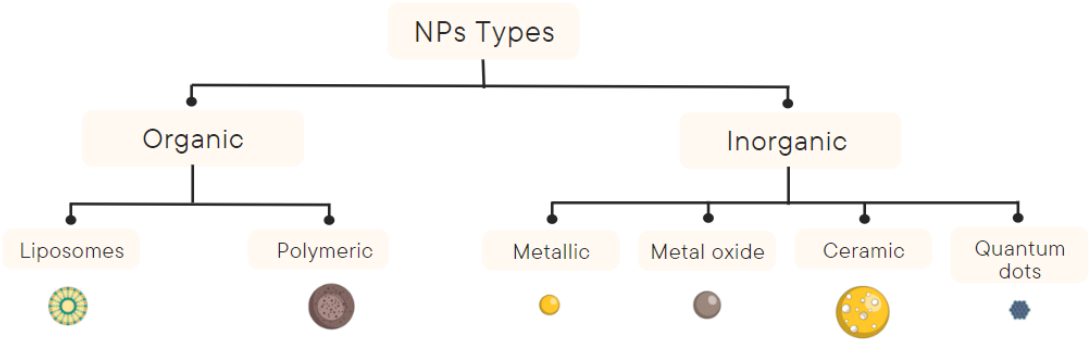


Figure 3 - Types of NPs in nanomedicine.

2.4.2 Overcoming the blood-brain barrier

Several drug candidates that have been shown to have significant pharmacological activity have failed in clinical trials due to their insufficient passage through the BBB. It should also be noted that this barrier has efflux pumps, mediating the efflux of harmful substances and drugs out of the brain, thus being a major obstacle to therapeutic success [50].

In recent decades, several strategies for drug delivery through the BBB have been explored, such as invasive methods as osmotic perturbation of the BBB and chemical perturbation of the BBB. The former has been explored since the 1970s, however, despite some positive reports, this approach has critical limitations such as its non-specificity and invasiveness, resulting, for example, in seizures. Chemical disruption requires intra-arterial vasoactive agents that cause

a temporary inflammatory reaction in endothelial cells. Despite many attempts, this technique shows conflicting results in clinical trials [62]. Both rupture techniques promote stress on the TJs so that these junctions loosen and consequently enable drug passage between endothelial cells in the BBB.

Also, non-invasive approaches have been explored such as converting water-soluble molecules unable to cross the BBB into liposoluble molecules. Despite the success of this technique in crossing the BBB, many times the therapeutic molecule loses affinity with its target receptor [63]. Despite the efforts to obtain techniques able to cross the BBB, there are still some challenges such as systemic cytotoxicity due to poor selectivity of the drugs, increased disruption of the BBB due to the drug entry route into the brain, and negligible brain penetration (1-4% for most CNS drugs) due to low permeability of the BBB and/or rapid elimination [46].

The use of nanotechnology-based systems such as NPs for drug delivery is a revolutionary strategy, as it offers the possibility of delivering drugs to local areas of the brain by active targeting [47]. In this approach NPs' surface can be modified by targeting moieties such as natural ligands, proteins, and antibodies with affinity for receptors that are overexpressed in BBB endothelial cells, thus allowing them to cross this barrier and reach the brain tissue [64]. Different targeting moieties have been explored to target the BBB, and the most prevalent targets for brain delivery are the receptors for the transport of transferrin [65], folic acid [66], insulin [67], and low-density lipoprotein [68]. Folic acid (FA) is well-explored due to its small size, high stability, and low cost [69]. Wei et al. (2018) constructed a model of liposomes modified with FA and dNP2 peptide for PTX delivery. A monolayer cell culture was used as an *in vitro* BBB model. Acid-cleavable FA accumulated at the tumor site through the interaction of FA and Folate receptor (FR). Due to the synergistic BBB transmigration effect of FA and dNP2, it led to an increase in the accumulation of drug-loaded liposomes in brain metastases. Finally, FA mediated the selection of FR-positive tumor cells at the brain metastasis sites after transmigration through the BBB [70].

The activity and organization of BBB are usually altered in GBM patients, often exhibiting a disturbed and highly permeable BBB known as the blood-brain tumor barrier (BBTB) [47]. However, the above-mentioned receptors are still overexpressed in the BBTB, thus NPs for active targeting are still a valid approach for brain delivery.

Other properties, such as surface charge, may represent an advantage when it comes to crossing the BBB, such as negatively or neutrally charged NPs, not disturbing the integrity of this barrier and presenting a longer half-life of blood circulation when compared to positively charged NPs [71].

2.4.3 Currently Developed NPs for Natural Compounds Brain Delivery in GBM

In the last years, several types of NPs have been developed for the delivery of different natural compounds for GBM therapy. In particular resveratrol, quercetin, curcumin, and camptothecin have been the most explored for NPs-mediated delivery. Table 2 summarizes the current advances in this field, presenting the most recent and developed work for each of the studied natural compounds for GBM.

Table 2 - Natural Compounds for GBM Therapy.

Compound Name	Type	Surface coating	Targeting moiety	Size (nm)	Surface charge	Studied Models	Results	Ref.
Asiatic Acid	PLGA NPs	PVA	Tf	149	Negative	Human GBM cells (U87)	- Tf increased NPs internalization into U87 cells when compared to unmodified NPs.	[72]
Curcumin	Zein NPs	Polydopamine	G23 peptide	120	Negative	Rat glioma cells (C6)	- Induce cell death by apoptosis and oxidative stress and inhibit cell proliferation and migration. - G-23 modification increased the NPs' ability to penetrate the tumor tissue by almost 2-fold when compared with unmodified NPs.	[73]
Betulinic Acid	Self-assembled	PVA	n.a.	60	Negative	Intracranial GBM tumor-bearing mice	- Increase the survival benefit when compared with free BA and standard treatment, with a reduction of tumor size. -Decrease the number of proliferative tumor cells.	[59]
Cardamom	Gelatin NPs	Polysorbate 80	n.a.	212	Negative	Human GBM cells (U87)	- Induce apoptosis more significantly than free cardamom.	[74]
Resveratrol	PCL NPs	PEG	Pep-1	30	n.d.	Rat GBM cells (C6) subcutaneous GBM tumors-bearing rat	- Tumor-inhibitory effect. - Pep-1 significantly increases cellular absorption and antiproliferative effects.	[75]

Camptothecin	PLGA NPs	PVA	n.a.	206	Negative	Intracranial GL261 tumors in immune competent C57 albino mice	- Slow tumor growth with a mean survival of 36.5 days. -Delivery of larger amounts of drug without adverse effects	[76]
Quercetin	PMMs	E-TPGS Poloxamer 407 Soluplus	n.a.	107.2	Negative	Rat glioma cells (C6) Human GBM cells (U87)	-Increase by 2-fold the cellular absorption and by 1.7-fold the values of IC50 when compared with free Qu.	[77]
Genistein and Temozolomide	PLGA NPs	n.a.	n.a.	135.5	Positive	Human GBM cells (U87)	-25% reduction in U87MG cell viability after 48h treatment -30% reduction of wound healing after 48h treatment.	[78]
Gallic Acid	Gold NPs	n.a.	n.a.	23	n.d.	Human GBM cells (U251)	-Decrease the survival of tumor cells when combined with radiation. -32% of tumor cell death when combined with radiation.	[43]
Melatonin	PCL NPs	Tween 80	n.a.	166	Negative	Human GBM cells (U87) Male Wistar rats	-Improved cell death when compared with free GA -NPs accumulate in the brain tissue after intranasal administration	[79]
Kaempferol	Egg-lecithin nanoemulsion	Chitosan and polysorbate 80	n.a.	145 180	Negative Positive	Rat glioma cells (C6) Male Wistar rats	- Chitosan improved KPF accumulation in the brain. - Decrease tumor cell viability. - Cytotoxicity in GBM is 20 times higher than free drug.	[80]

Abbreviations: poly(lactic-co-glycolic acid) (PLGA); transferrin (Tf); glioblastoma (GBM); immortalized human astrocytes (NHA); Blood-brain barrier (BBB); Vitamin-E polyethyleneglycol-1000 succinate(E-TPGS); solid lipid nanoparticle (SLN); poly(ethylene glycol)-b-poly(caprolactone) (PEG-b-PCL); polymeric mixed micelles (PMMs); epigallocatechin-3-gallate (EGCG); camptothecin (CPT), non-applicable (n.a.), non-disclosed (n.d).

1) Asiatic Acid

Ramalho et al. (2022) developed transferrin (Tf)-conjugated polylactic-co-glycolic acid (PLGA) NPs for the encapsulation of asiatic acid (AA). The nanosystem was evaluated *in vitro* using human GBM cells (U87) and healthy brain cells as control (immortalized human astrocytes) [72]. The results showed that the functionalization of PLGA NPs with Tf molecules significantly improved the cellular uptake in GBM cells in two different treatment periods (0.5 and 2 hours). Additionally, the authors proved that the internalization of the Tf-modified NPs occurs by TfR-mediated endocytosis, by showing that blocking the TfR with Tf excess decreased the NPs' uptake by 68 ± 1%. *In vitro* cytotoxicity studies revealed that AA encapsulation did not alter its therapeutic potential. Though, surface modification with Tf increased the IC50 values from 80 ± 2 μM to 130 ± 18 μM, due to a slower compound release from the NPs. However, the authors expect to prove in future *in vivo* studies that surface modification with Tf will enable the NPs selectivity and bioaccumulation of the natural compound in the tumor tissue.

2) Curcumin

Zhang et al. (2021) developed zein NPs for the delivery of curcumin (CUR) for GBM therapy. The NPs surface was coated with polydopamine to improve its colloidal stability and it was also modified with a peptide (G23) with a well-proven ability to cross the BBB [73]. The nanoformulation was evaluated *in vitro* using a BBB model composed of human brain endothelial cells (hCMEC/D3 cells) and a model of rat glioma cells (C6). To evaluate the *in vitro* BBB targeting ability, the NPs were modified with a fluorescent marker (coumarin 6). The results showed that the G23 peptide improved the transcytosis after 8 hours of incubation, with about 16.9 ± 2.2% of G23-modified NPs crossing the BBB model and only 9.6 ± 1.5% and 7.8 ± 1.8% for free C6 and unmodified NPs, respectively. *In vitro* experiments using 3D models of cell spheroids revealed that G-23 modification increases the NPs' ability to penetrate the tumor tissue by almost 2-fold when compared with unmodified NPs. Furthermore, the results showed that CUR encapsulation improved its ability in inducing cell death by apoptosis and oxidative stress and in inhibiting cell proliferation and migration. Interestingly, the surface modification with the G23 peptide did not show improved efficacy when compared with non-modified NPs.

3) Betulinic Acid

Li et al. (2022) prepared betulinic acid (BA) self-assembled NPs to compare the antiproliferative activity of free BA and BA NPs in GBM cells [59]. In a previous study, the authors demonstrated that BA self-assembles into rod-shaped NP that can target the brain tissue in a mice model [81]. Now, this work evaluated the efficacy of these NPs for glioma treatment *in vivo* using intracranial tumor-bearing mice. The animals were grouped and received treatment of PBS, TMZ, free BA, or BA NPs (20 mg/kg of BA 3 times per week). After

3 weeks of treatment, it was found that compared to the group receiving PBS, the survival of the mice receiving free BA and TMZ group was significantly increased, accompanied by a decrease in the tumor size. Furthermore, the administration of BA-NPs further increased the tumor growth inhibition and survival benefit when compared with TMZ and free BA. In addition, no toxicity was observed in major organs, suggesting that intravenous administration of BA-NPs has limited systemic toxicity is a safe and effective approach to inhibit GBM tumor development [59].

4) Cardamom

The study conducted by Nejat et al. (2017) had as its main objective the production of cardamom-loaded gelatin NPs as a potential delivery nanosystem for the treatment of GBM [74]. The NPs were coated with polysorbate 80 due to its ability to cross the BBB. The authors further evaluated the cytotoxic effects of the developed nanoformulation *in vitro* using human GBM cells (U87). The cardamon-loaded NPs showed a higher level of apoptosis for GBM cells treated with cardamom-loaded NPs when compared to the free compound. These results support the possible applicability of cardamom-containing nanosystems for treating GBM effectively.

5) Resveratrol

In this study by Lin et al. (2021), resveratrol (RES) was loaded in poly (caprolactone) (PCL) NPs coated with PEG and functionalized with Pep-1 peptide with GBM tumors targeting ability [75]. The developed nanoparticles were evaluated *in vitro* using rat glioma cells (C6). Fluorescence microscopy and flow cytometry studies both revealed that Pep-1 modification enhanced cell uptake when compared with control unmodified NPs. Furthermore, resveratrol loaded in Pep-1 NPs showed higher antiproliferative effects in C6 cells than resveratrol in the free form or loaded in non-modified NPs, which exhibited similar effects. Also of note, blank NPs showed no toxicity to healthy brain cells.

In vivo experiments were performed in rats bearing subcutaneous tumors. The animals were either treated with saline as control, free RES, RES loaded in Pep-1-modified NPs and RES loaded in unmodified NPs) with three administrations at two-day intervals for 12 days. The suppressive effect of free RES on the tumor was weak, in contrast to the effect exhibited by RES-NPs and especially Pep-RES-NPs. Overall, the results confirmed the anti-GBM effects of both nanoformulations without affecting healthy brain cells.

6) Camptothecin

Householder et al. (2015) developed PLGA NPs for the delivery of camptothecin (CPT) and evaluated their ability to treat intracranial GBM-bearing mice [76]. The efficacy of CPT in loaded in NPs versus free form was evaluated after weekly intravenous injections of saline, free

CPT, NP-10 (PLGA NPs at a CPT dose of 10 mg/kg), or NP-20 (PLGA NPs containing CPT at 20 mg/kg) for 3 weeks. When treated with NP-20, tumor growth was significantly slowed and showed a survival benefit over the other groups (mean survival of 36.5 days compared to 28, 32, and 33.5 days for saline, free CPT, and NP-10 respectively).

Histological analysis of the tumor tissue collected from mice treated with NP-20 showed an increase in biomarkers for DNA damage compared to free CPT. The results support the hypothesis that encapsulation of CPT in NPs allows the delivery of larger amounts of CPT to the tumor tissue.

7) Quercetin

Paranthaman et al. (2022) developed polymeric mixed micelles (PMMs) for the encapsulation of quercetin (Qu). Three-level Box-Behnken Design (BBD) was used to optimize the PMMs (Soluplus, E-TPGS, and poloxamer 407). The nanosystem was evaluated *in vitro* using human glioblastoma cells (U87MG) and mouse glioma cells (C6) [82]. The results showed that the IC50 values were about 1.7 times higher for this nanoformulation in both cell lines compared to the free drug. The percentage of cellular uptake was 2.12 and 2.41 times higher than the free drug in C6 and U87MG cells, respectively. Finally, Qu encapsulation showed better performance in all aspects of this study. The authors hope to extend this work in the future to improve blood-brain barrier penetration.

8) Genistein and TMZ

Meteoglu and Erdemir (2021) developed PLGA NP for the encapsulation of temozolomide (TMZ) and genistein (Gen). The nanoformulation was evaluated *in vitro* using U87MG human glioblastoma cells [78]. The cytotoxicity of Gen-NPs, TMZ-NPs, and Gen-TMZ-NPs on tumor cells was also evaluated, and after 24 and 48 hours treatment with TMZ-NPs and Gen-NPs, no significant change in U87MG cell viability was observed. On the other hand, treatment with Gen-TMZ-NP significantly decrease the U87MG cell viability in a dose- and time-dependent manner, resulting in a 25% reduction in U87MG cell viability after 48 hours treatment with Gen-TMZ-NPs (100 µg/mL). Furthermore, encapsulation of TMZ and Gen in PLGA NPs increased the solubility and stability of the molecules, thereby increasing cytotoxic activity in U87MG cells.

The effect of Gen-TMZ- PLGA NPs on the proliferation and migration of U87MG cells demonstrated a wound closure rate of 30.59% after 48 hours. Furthermore, in the Gen-TMZ-NP treated group, after 48 hours, the wound closure rate was 6.80%, thus revealing the most significant inhibition in cell migration activity. Finally, the results also showed an increased expression of intrinsic apoptosis proteins in the glioblastoma cells treated with Gen-TMZ-NPs.

9) Gallic Acid

In this study, Jing et al. (2021) encapsulated gallic acid (GA) in gold NPs and evaluated their effects on viability and radiation sensitization in human GBM cells (U251) [43]. U251 cells were treated with increasing concentrations of GA-NPs (100, 150, 200 μg/mL) for 24, 48, and 72 hours. The NPs showed a significant cytotoxic effect on tumor cell survival that also proved to be time and dose-dependent. 3 days of treatment with 200 μg/mL GA-NPs decreased cell survival by about 30%. To evaluate whether GA-GNPs could sensitize GBM cells to radiation, cells were treated with a combination of different radiation doses (0, 2, 4, 6, 8, 10, and 12 Gy) and GA-NPs (100, 150, and 200 μg/mL) for 48 hours. The results showed significant survival differences for the higher concentrations of GA-NPs in combination with radiation when compared to radiation alone, demonstrating that GA-NPs can sensitize tumor cells to radiation [43]. Furthermore, it was demonstrated found that in the presence of radiation, cell death is more significant when treated simultaneously with GA-GNPs (32.7%) than with free gallic acid (28.3%) or control blank NPs (24.8%).

10) Melatonin

Junior et al. (2019) developed polycaprolactone (PCL) NPs for the nose-to-brain delivery of melatonin (MLT) to treat GBM [79]. The NPs were coated with Tween 80 to enhance the NPs penetration through the nasal mucosa. Cellular experiments were performed on human GBM cells (U87MG) and in control healthy fibroblasts (MRC-5 cells). Both cells were treated with free MLT, MLT-NPs, or blank-NP as control. After 48 hours, free MLT did not reduce cell viability in either group, and MLT-NPs promoted a significant decrease in GBM cell viability when compared to healthy fibroblasts. A 50% inhibition of tumor cell survival was observed for a concentration of 0.1 μg/mL of MLT in NPs.

The *in vivo* biodistribution of the NPs after intranasal administration was evaluated in healthy animals (male Wistar rats). For NPs visualization, these were loaded with a fluorescent marker (IR780). The acquired results demonstrated that MLT-NPs are appropriate to reach the brain after intranasal administration, allowing the increase of MLT concentrations in the brain and acting as a promising formulation for GBM treatment.

11) Kaempferol

This study, conducted by Colombo et al. (2018), aimed to prepare kaempferol (KPF)-containing lipid nanoemulsions (NE) to investigate the brain delivery potential after intranasal administration and to evaluate their antitumor activity against glioma cells [80]. Chitosan was used to coat the NPs due to its mucoadhesive properties. The results obtained from the *ex vivo* permeation study using porcine nasal mucosa allowed to realize that chitosan-modified KPF-NE exhibited higher permeation (13.04 ± 1.97 μg/cm^2) compared to free KPF (5.79 μg/cm^2) and non-modified KPF-NE (5.72 μg/cm^2). The biodistribution of KPF after intranasal administration

in healthy animals (Wistar rats) was also investigated, and the concentration of the compound in the brain tissue was significantly higher when loaded in the chitosan-modified NE than in KPF-MNE when compared to free KPF solution and nonmodified NPs. Additionally, rat C6 glioma cells were treated with KPF in the free form or loaded in chitosan-modified and unmodified NE and chitosan-NPs exhibited a more significantly decreased tumor cell viability when compared to the other treatment groups. The cytotoxicity of KPF-chitosan-NE was about 20 times higher than free KPF due to the observed higher *in vitro* cellular uptake in C6 cells when KPF is loaded into the mucoadhesive nanoemulsion. Finally, despite the mucoadhesive formulation being able to inhibit cell growth in rat glioma cells, it did not alter DNA content after treatment, indicating that it didn't disturb the cell cycle progression.

Chapter 3

Materials and Methods

3.1 Materials

Polyvinyl alcohol 4-88 (Mowiol ® 4-88, MW 31,000) (PVA), PLGA Resomer® RG 503 H (50:50; MW 24,000 – 38,000), 1-ethyl-3-(3-dimethylaminopropyl) cardodiimide (EDC) (MW 191.70), folic acid (FA) (≥97%, MW 441.40), gallic acid (GA) (97.5-102.5%, MW 170.12), phosphate-buffered saline (PBS) and acetic acid (≥ 98%, MW 60.05) were purchased from Sigma Aldrich (St. Louis, MO, USA). Ethyl acetate (EA) (99.6%, ACS reagent, MW 88.11) was acquired from BioVision (Waltham, MA, EUA). Trypsin (Gibco™ TrypLE™) and fetal bovine serum (Gibco™ FBS) were purchased from Fisher Scientific (Hampton, NH, USA). High-glucose Dulbecco's Modified Eagle medium (DMEM) was purchased from Capricorn Scientific (Ebsdorfergrund, Germany). Penicillin-Streptomycin solution (x100) and funzigone were purchased from Biowest LCC (Riverside, MO, USA). Trypan blue (≥ 70%, MW 960.80) was purchased from Biochem Chemopharma (Cosne-Cours-sur-Loire, France). Trichloroacetic acid (TCA) (99%, MW 163.38). Tris(hydroxymethyl)aminomethane (≥ 99.8%, MW 141.14),and Sulforhodamine B (SRB) (MW 580.66) were purchased from Sigma-Aldrich (St. Louis, MO, USA). Dimethyl sulfoxide (DMSO) (≥ 99.9%, MW 78.13) was purchased from VWR international (Radnor, PA, USA).

3.2 Preparation of the Gallic Acid-loaded PLGA NPs

The GA-loaded NPs were produced using the single-emulsion evaporation method. For that, 1.0 mg of GA and a known amount of PLGA were dissolved in ethyl acetate. The choice of ethyl acetate as solvent was based on preliminary solubility and stability tests, presented in Appendix A3. To this organic solution, 2.0 mL of an aqueous solution of polyvinyl alcohol (PVA) was added dropwise. The preparation was emulsified by mechanical agitation using the vortex for 30 sec. Next, the emulsion was subjected to 10-sec on/off sonication cycles with an amplitude of 70% and a frequency of 24 kHz (probe sonicator, UP400S, Hielscher, Berlin, Germany). The emulsion was quickly transferred to a beaker and placed on a magnetic stir plate at 800 rpm (revolutions per minute) (Colosquid, ika®, electromagnetic stirrer) until complete evaporation of the organic solvent. The suspension of NPs was kept in the refrigerator at 4 ºC for 2 hours to stabilize.

After 2 hours, the NPs were collected by centrifugation and resuspended in 1.0 mL of ultrapure water. The supernatant was saved for non-encapsulated drugs quantification. During centrifugation, the rotation time and speed were increased gradually. Thus, the time values ranged from 2 min to 1 hour and the speed ranged from 5000 to 14500 rpm.

3.3 Functionalization of GA-PLGA NPs with Folic Acid

The conjugation of FA to the surface of NPs was achieved through the crosslinking reaction of the terminal carboxylic group of PLGA with the primary amine of FA, mediated by 1-ethyl-3-(3-dimethylaminopropyl) carbodiimide (EDC). To this end, an aqueous solution of EDC was prepared at 1.0 mg/mL. EDC is one of the most widely used carbidiamides to catalyze bond formation between carboxylic and the amine groups [83]. Figure 4 represents the chemical reactions between FA and nanoformulations using EDC.

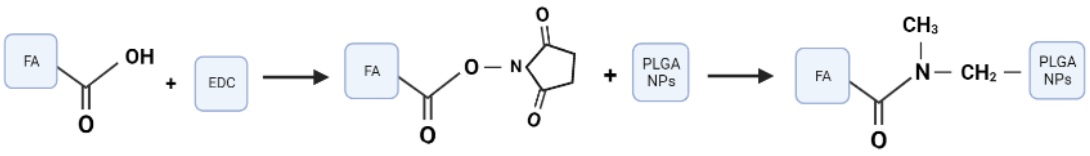


Figure 4 - Chemical reactions between FA and polymeric NPs catalyzed by EDC.

A molar excess (approximately 20-fold) of EDC was added to the NPs and incubated at room temperature for 30 min on a stir plate (Colosquid, ika®, electromagnetic stirrer). Then, a molar excess of FA was added to the suspension of NPs with the activated carboxylic group and

incubated at room temperature for 1 hour with mechanical shaking. The NPs were collected by centrifugation as mentioned in the previous section and resuspended in ultrapure water.

3.4 Experimental Design and Protocol Optimization

An Experimental Design was implemented to optimize the production of the NPs, as an alternative to the traditional technique of one factor at a time (OFAT) since, unlike the latter, it allows the optimization of the protocol associated with the preparation of NPs by systematically and simultaneously changing the experimental parameters [84]. In addition, it is a fast and effective technique, since the variables are changed systematically and statistical optimization is used, allowing a simple data analysis [85]. Thus, depending on the objectives to be achieved, there is a set of models that can be applied, varying in the quality of information obtained and the number of experiments to be performed [86]. The choice of the appropriate model is preponderant for obtaining reliable results. To optimize the experimental protocol used in this work, the Central Composite Design (CCD) model was applied. The CCD allows obtaining results in a precise way, through the construction of a second order quadratic model, capable of examining each factor in five distinct levels, allowing the estimation of the quadratic terms [87]. This model is inserted in the response surface analysis, where the models are capable of plotting contours in more than one dimension, to describe the response through quadratic or cubic equations. In this way, the relationship between the different parameters is presented in the form of polynomials with curvature and can go beyond linearity [88].

In this work, the Design Expert software (version 11.1.2.0, Stat-Ease Inc., Minneapolis, USA) was used to implement the model. The experimental parameters (independent variables) were chosen and varied as presented in table 3, thus representing the most preponderant variables for the preparation of the NPs. According to the used model, these parameters were varied in five levels: -1, -α, +1, 0, and +α, with |α| assuming a value of 1.54671. The α value is set considering the calculations that will be performed, and the accuracy required for the response being automatically determined by the software after choosing an orthogonal quadratic design with three center points [89]. The independent variables chosen were the amount of PLGA, the percentage of PVA, the number of FA molecules per NP, and the number of sonication cycles.

Table 3 - Independent variables and varying levels used in the experimental design.

Parameters	Component	Units	Applied Level				
			-α	**-1**	**0**	**+1**	**+α**
A	m_{PLGA}	mg	1.8	10	25	40	48.2
B	PVA	%	0.18	1	2.5	4	4.82

C	FA molecules/ NP	unit	18	100	250	400	482
D	sonication cycles	unit	1	2	4	6	7

Note: m_{PLGA} - PLGA mass; PVA – percentage of PVA; FA molecules/NP - number of folic acid molecules per nanoparticle; sonication cycles – number of sonication cycles of 10 seconds each.

The responses (dependent variables) under study were the size of the NPs, the polydispersity index (PDI), the zeta potential, and the encapsulation efficiency (EE) of GA. According to the model, the software proposed the preparation of 27 nanoformulations, 3 of them corresponding to center points, which allow to evaluate the experimental reproducibility, to fit quadratic polynomials [85]. Then, the experimental design was augmented, by preparing 3 additional center points, to obtain a better statistical analysis by the software. To avoid bias, the order of the formulations was set randomly. Below, in table 4, the summary of the experimental design and the responses obtained are presented.

Table 4 - Experimental design and obtained responses of all 30 nanoformulations. The experimental levels (low, center, high, and alpha) are represented by -1, 0, +1, and α, respectively.

Run order	Coded independent variables							
	A	**B**	**C**	**D**	**Mean diameter (nm)**	**PDI**	**Zeta Potential(mV)**	**EE GA (%)**
1	-1	-1	-1	-1	158.3	0.039	-6.6	21.6
2	+1	-1	-1	-1	181.1	0.036	-10.3	34.8
3	-1	+1	-1	-1	181.0	0.052	-20.5	47.0
4	+1	+1	-1	-1	158.4	0.028	-22.9	47.0
5	-1	-1	+1	-1	158.3	0.065	-15.1	23.3
6	+1	-1	+1	-1	195.6	0.05	-18.5	28.1
7	-1	+1	+1	-1	143.8	0.063	-13.3	57.4
8	+1	+1	+1	-1	153.9	0.051	-23.4	44.4
9	-1	-1	-1	+1	143.9	0.056	-7.1	13.0
10	+1	-1	-1	+1	174.1	0.041	-8.9	34.5
11	-1	+1	-1	+1	130.4	0.081	-15.5	47.4
12	+1	+1	-1	+1	135.2	0.026	-20.5	55.1
13	-1	-1	+1	+1	167.7	0.062	-13.4	17.9
14	+1	-1	+1	+1	193.8	0.117	-19.6	16.8
15	-1	+1	+1	+1	113.0	0.062	-12.6	62.2
16	+1	+1	+1	+1	121.0	0.048	-20.6	50.6

17	- α	0	0	0	193.1	0.333	-19.4	48.8
18	+ α	0	0	0	163.6	0.088	-21.2	54.2
19	0	- α	0	0	371.8	0.115	-23.3	24.7
20	0	+ α	0	0	140.0	0.098	-18.9	62.0
21	0	0	- α	0	145.2	0.057	-21.4	44.2
22	0	0	+ α	0	139.8	0.058	-19.9	56.3
23	0	0	0	- α	171.5	0.028	-22.0	41.4
24	0	0	0	+ α	143.0	0.075	-19.1	60.1
25	0	0	0	0	154.9	0.034	-19.6	43.2
26	0	0	0	0	141.9	0.061	-17.5	27.5
27	0	0	0	0	140.3	0.053	-22.2	28.1
28	0	0	0	0	155.2	0.043	-19.0	40.7
29	0	0	0	0	160.0	0.037	-19.5	46.1
30	0	0	0	0	156.4	0.036	-19.4	48.8

For the statistical analysis of the model, analysis of variance (ANOVA) was used, which determining the significance between the independent variables or interactions between them by comparing the responses obtained and the variance of the associated error [88]. Thus, the mathematical regression model was adjusted, and p-values of less than 0.05 were considered significant, with a 95% confidence interval.

3.5 NPs Physicochemical Characterization

The size (nm), polydispersity index (PDI), and zeta potential (mV) of the produced NPs were assessed for their physicochemical characterization. The ZetaSizer Software examined the acquired data (version 8, Malvern Instruments, UK).

3.5.1 Dynamic Light Scattering

Dynamic Light Scattering (DLS) is a technique defined by measuring the Brownian motion of macromolecules that are in suspension [90]. This technique is widely used in measuring the size of NPs and for evaluating their colloidal stability over time [58]. Brownian motion is defined as the random motion of particles originating from their collision with solvent molecules [91].

Characteristics such as particle size, temperature, and viscosity of the medium are important when performing this technique since the particle motion is dependent on them. Thus, it is necessary that, when performing DLS measurements, the temperature is known, whereas the viscosity of the dispersant is closely related to it [90].

Through the random motion of the particles in each period (Brownian motion), it is possible to obtain information regarding the size of the particles since they are closely related. Given

the continuous motion of the particles, the light incident on them undergoes a phenomenon called Doppler broadening. The intensity fluctuations of the scattered light depends on the diffusion rate of the particles, i.e., the smaller the particle, the faster it moves, translating into faster fluctuations of scattered light and vice versa [91].

The rate of Brownian motion is quantified by the translational diffusion coefficient (D). Thus, after determining the diffusion coefficient of the molecules, other parameters, such as the hydrodynamic radius (R_h), can be measured by applying the Stokes-Einstein equation:

$$D_\tau = \frac{k_B T}{6\pi\eta R_h} \qquad (1)$$

Where k_B is the Boltzmann coefficient (1.380×10^{-23} $kg.m^2.s^{-2}.K^{-1}$), T is the absolute temperature and η is the viscosity of the dispersant [91].

The determined hydrodynamic size is larger than the actual particle's radius since the ion layer that moves with it is also considered. Another parameter that is obtained in this measurement is the polydispersity index (PDI), which indicates the monodispersity tendency of the sample, allowing to understand what is the "range" of particle size distribution [73,74]. In a monodisperse sample, the ideal value of the PDI is below 0.1 [51].

The size and PDI of the NPs were measured by DLS using a ZetaSizer Nano ZS (Malvern Instruments, UK). The NPs were diluted in ultrapure water (1:10) to a final concentration of 1 mg/mL. The samples were analyzed with a 633 nm red laser at 25 ºC with an angle of 173°, and the results obtained were given by the intensity distribution.

3.5.2 Laser Doppler Velocimetry

The zeta potential (ζ) is defined as the potential of a particle moving in an electric field in the shear plane (slipping plane). The zeta potential reflects the potential difference between the electron double layer of the electrophoretically moving particles and the dispersant layer that exists around them in the shear plane [92].

When a particle is in suspension, an adsorption double layer forms on the surface. As depicted in Figure 5, the innermost layer, also called the Stern layer, is composed essentially of ions of opposite charge to the molecule tightly coupled to the nucleus [92]–[94]. After this layer, the electrostatic effect decreases. After the Stern layer, there is another, diffuse layer composed of charges equal and opposite to the Stern layer. This phenomenon is due to the electrostatic field that is present. Thus, when an electric field is applied to such a dispersion, the particles that are charged move toward the oppositely charged electrode (electrophoresis) [92].

Within the diffuse layer, there is a hypothetical plane that acts as an interface between the moving particles and the surrounding dispersant layer. This plane is called the shear plane and the zeta potential is the potential that exists at this interface [92]–[94].

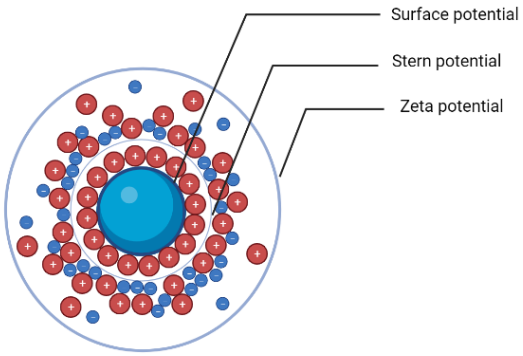


Figure 5 - Representation of the electric double layer.

Because the zeta potential cannot be measured directly, it is deduced from the electrophoretic mobility (μ_e) when an electric field is applied to the sample. The electrophoretic mobility can be calculated using the following equation: [93]

$$\mu_e = \frac{v}{E} \qquad (2)$$

After calculating the electrophoretic mobility, it becomes possible to determine the zeta potential value (ζ) using the Helmholz-Smoluchowshi equation: [93]

$$\mu_e = \frac{\varepsilon\zeta}{4\Pi\eta} \qquad (3)$$

In this equation, ε the dielectric constant in vacuum, and η the viscosity coefficient of the dispersant [92].

Zeta potential measurements were also performed using the ZetaSizer Nano ZS (Malvern Instruments, UK) in a DTS1060 cell. The NPs were diluted in ultrapure water (1:10), obtaining a final concentration of NPs equivalent to 1 mg/mL. The zeta potential values were obtained by the Smoluchowski model using the dielectric constant (78.5), refractive index (1.330), and viscosity (0.8872 cP) of water as the dispersant at room temperature. The data obtained were analyzed by ZetaSizer software (version 8, Malvern).

3.6 Determination of Encapsulation Efficiency

The encapsulation efficiency (EE) of the produced NPs was determined indirectly by quantifying the non-encapsulated GA. EE is defined as the amount of drug encapsulated in the NPs relative to the total amount of drug added during the encapsulation process, expressed as a percentage [95]. The supernatant containing the free compound was separated as described in section 3.3. The absorbance of the supernatant obtained after functionalization with FA was

also measured to quantify the GA that might be eventually lost in the functionalization process. Free GA was quantified by the UV-vis absorbance spectra at a wavelength of 261 nm using a microplate reader (Synergy 2 Microplate Reader, BioTek, UK). The obtained absorbance values were correlated to a GA calibration curve in PVA (figure A1.1, Appendix A1).

The EE (%) values for GA were determined using the following equations:

$$Encapsulated\ GA\ (mg) = total\ GA\ (mg) - (non - encapsulated\ GA\ (mg) + GA\ lost\ in\ functionalization\ (mg)) \quad (4)$$

$$EE\ (\%) = \frac{encapsulated\ GA\ (mg)}{total\ amount\ of\ GA\ (mg)}\ 100 \quad (5)$$

3.7 Fourier-Transformed Infrared Spectroscopy

Attenuated Total Reflectance Fourier-Transformed Infrared Spectroscopy (ATR-FTIR) was used to confirm the FA conjugation onto the GA-PLGA NPs. FTIR is an effective tool for identifying material chemistry with high spectral resolution and a wide frequency range [96] and has been the most useful approach for monitoring NPs' surface functionalization since it is simple to use and uses a non-destructive testing method [97].

A Bruker Alpha-P FTIR Spectrometer (Bruker Optics Inc., Billerica, MA, USA) and Opus Software (version 6.5, Bruker Optik GmbH) were used to record the FTIR spectra of the produced NPs. The spectra were attained in absorbance mode with 64 scans at a resolution of 4 cm^{-1} for both the sample and background observations and a wavenumber range of 4000-375 cm^{-1}. The acquired spectra's intensity range was normalized and smoothed using Graphpadprism (version 9.1.2, GraphPad Software). A 10 µL drop of each sample was deposited on the crystal for examination, and it was then dried with a nitrogen flow. FTIR measurements were made for FA stock solution, PLGA NPs, GA-loaded PLGA NPs, and FA-GA-loaded PLGA NPs.

3.8 Transmission electron microscopy (TEM)

Transmission electron microscopy (TEM) is a microscopy technique widely used in nanomedical research that allows obtaining detailed images with high resolution of the sample under study, through the transmission of an electron beam in a thin sample [98]. To perform this technique, the prepared FA-GA-loaded NPs were placed on copper grids (Formvar/Carbon - 400 mesh Copper, Agar Scientific, UK) and negatively stained with 2% (v/v) uranyl acetate. In TEM, the scattering of electrons in the sample causes a contrast between the different structures depending on the number of electrons scattering. To increase this contrast, heavy metal salts are used since they easily interact with the electron beam [99]. Uranyl acetate is

a salt of the metal uranium commonly used in TEM, where uranyl ions combine in large quantities with the phosphate groups of nucleic acids. Its use provides good contrast, allowing for easier visualization and analysis of the sample under study [100].

For sample preparation, an over grid was used where 5 µL of the suspension of NPs was soaked in it over 5 minutes. Next, the grid was stained with uranyl acetate for 45 seconds. Finally, the sample was air-dried before visualization. The NPs were visualized with an accelerating voltage of 80 kV using a Jeol JEM 1400 electron microscope (Japan). At least three images were acquired.

3.9 *in vitro* Release Experiments

The *in vitro* release profile of GA by FA functionalized NPs was determined over the course of 15 days under simulated physiological conditions. Two releases were performed, where the difference between the two was centered on the pH present in Phosphate Buffered Saline (PBS). PBS is an isotonic buffer widely used in biological applications, as it can mimic the pH, osmolarity and ionic concentrations of the human body, and shows no toxicity [101]. First the NPs were suspended in 3 mL of PBS (0.01 M, pH 7.4) at 37°C, to be divided into 10 aliquots. The second release was performed in the same way, but simulating a pH of 6.4, since the pH present in tumor tissues is between 6.2-6.8 [102], while pH 7.4 corresponds to blood/health tissues pH [103]. Also, the solubility of the drug in each of the medium was also verified.

Thus, at each timepoint, to separate the NPs from GA released, the aliquots of the NPs were centrifuged. Through the supernatant obtained it is possible to determine the amount of drug released over time, by measuring UV-Vis absorbance (UV-1700 PharmaSpec UV-Vis spectrophotometer, Shimadzu, Japan). The absorbance values were correlated with a control sample containing GA.

Finally, the GA release curve was plotted using the equation below, revealing the percentage of GA released over time.

$$\%\ GA_{release}\ \frac{amount\ of\ GA\ released\ \ at\ time\ t}{amount\ of\ encapsulated\ GA} \times 100 \qquad (6)$$

3.10 Evaluation of NPs' Stability

To evaluate the stability of GA-loaded NPs functionalized with FA, the size (nm), PDI and zeta potential (mV) were measured using the DLS technique. Note that the colloidal stability the optimal nanoformulations was evaluated under storage conditions at 4°C in weekly measurements for 6 weeks. In addition, and to simulate physiological conditions (37ºC, 0.01 M),

the stability of these nanoformulations was also measured in two different pH: 6.4 to simulate tumor tissue and 7.4 to simulate blood pH, over 2 weeks.

3.11 Cell Culture

To analyze the cytotoxicity of the optimal NPs produced, two different cell lines were used: the U251 line, a GBM tumor cell line, and a healthy cell line - the normal human astrocytes (NHA) line as control. For this, both cell lines were cultured in Dulbecco's Modified Eagle Medium (DMEM) supplemented with 10% FBS. 1% penicillin-streptomycin and 1% fungizone were added to the culture to decrease the probability of contamination. For cell passage, the cells were trispsinized to detach them from culture flasks. Throughout the experimental work the cultures were kept at 37 ºC in an incubator with 5% CO2.

3.12 Sulforhodamine B assay

To test the effect of GA-loaded NPs functionalized with FA, the colorimetric assay with sulforhodamine (SRB) was used, for both cell lines (U251 and NHA). In this cellular assay, free GA and PLGA NPs without the addition of the drug were also tested to compare their therapeutic efficacy compared to drug-loaded NPs. The SRB cell viability assay is usually used due to its simplicity, precision, and reliability, since through the interaction of the SRB dye with the amino acids present in the cell proteins, it is possible to quantify the number of viable cells [104].

For this assay, 96-well plates were used, with cells grown at a density of 1000 cells per well. The cells were incubated at 37º C for 24 hours in a humidified incubator at 5% CO_2 for cell adhesion. Then the free drug, FA-GA-loaded NPs and PLGA NPs were diluted in DMEM medium and added to the cells. The GA concentrations used were as follows: 0.1- 1000 µM for free GA and 10-3000 µM for the FA-GA-loaded NPs. Control NPs were added at a PLGA concentration of 0.18-0.72 mg/mL. The remaining cells were used as controls and were not treated. The cells were then incubated, over 72 hours, and the SBR protocol was subsequently performed. For this assay it was necessary to use 10% (w/v) trichloroacetic acid (TCA), previously prepared, at 4º C for 1 hour, to fix the cells. After the desired time, the cells were washed and dried in the 37º C oven. Next, 50 µL of SRB (0.4 % in 1% acetic acid) was added to each well and allowed to stain the cells for 20 minutes. To remove the excess dye that was not incorporated, the samples were washed twice with 200 µL of 1% (v/v) acetic acid and dried in the oven at 37º C. Finally, 100 µL of Tris buffer solution (10 mM) was added to solubilize the incorporated dye and allow the consequent absorbance reading. Protein quantification was measured using UV-Vis absorbance (BioTek Synergy HT Microplate Reader - BioTek, UK) at 560 and 655 nm.

Cell survival was determined by the following equation:

$$Cell\ survival\ (\%) = \frac{\mathrm{T}}{C} \times 100 \quad (7)$$

Where T translates to the absorbance value of the treated cell wells and C to the absorbance value of the cell wells not treated with GA or NPs, i.e., the control.

The dose-response curves were plotted with GraphPad 9.3.1 software (GraphPad Software Inc., USA)

3.13 Statistical Analysis

The results presented are in the form mean ± standard deviation (SD) for the five independent optimal nanoformulations. The T-student test was used to compare the averages of the stability results and cell assays. This test was applied for statistical analysis, with a 95% confidence interval, and $p<0.05$ was considered significant.

Chapter 4

Results and Discussion

4.1 Experimental Design and Protocol Optimization

As mentioned in the methodology, the preparation protocol of GA NPs functionalized with FA was optimized by using DoE. Through preliminary experiments, four independent variables were identified and chosen as those preponderant for having direct effect on the physicochemical characteristics of the NPs: mass (mg) of PLGA (A), percentage (%) of PVA (B), number of FA molecules per NP (C) and number of sonication cycles (D). It should be noted that the other parameters present in the nanoformulations preparation protocol remained constant throughout their production. As dependent variables in study, the size of the NPs (Y_1), PDI (Y_2), zeta potential (Y_3) and GA EE (Y_4) were chosen, since these responses allow to infer about the possible internalization of the drug in the target tissue and about the amount of drug that was trapped in the formulations.

Thus, initially 27 nanoformulations, containing 3 replicates of central points, were prepared using the CCD model. After a first statistical ANOVA analysis, the model did not show to be significant ($p>0.05$) for the variables of PDI (Y_2) and GA EE (Y_4), so it was decided to augment the experimental design by adding 3 more central points. Subsequently, a second analysis was performed, which proved to be statistically significant ($p<0.05$) for all the chosen responses. For the first three dependent variables (size, PDI and zeta potential), the model chosen through the ANOVA statistical analysis was the quartic regression model and for the remaining (GA EE) linear regression model was chosen. Table 5 presents the results obtained through this statistical analysis, for all responses, which proved to be significant. The detailed summary of

each model applied to each of these parameters can be found in tables A2.1-A2.4 in Appendix A2.

Table 5 - Results of the statistical analysis using ANOVA.

Parameter			**Size – Y_1**		
	SS	dF	MS	F-Value	p-value
Model	5.69 X 10^4	24	2372.9	34.99	0.004
Residual					
Lack of Fit					
Pure Error	339.09	5	67.82		
Cor Total	5.72 X 10^3	29			
R^2	0.9941				
Parameter			**PDI – Y_2**		
	SS	dF	MS	F-Value	p-value
Model	0.089	24	0.0037	31.76	0.0006
Residual					
Lack of Fit					
Pure Error	0.0006	5	0.0001		
Cor Total	0.0896	29			
R^2	0.9935				
Parameter			**Zeta – Y_3**		
	SS	dF	MS	F-Value	p-value
Model	638.18	24	26.59	11.42	0.0065
Residual					
Lack of Fit					
Pure Error	11.65	5	2.33		
Cor Total	649.83	29			
R^2	0.9821				
Parameter			**EE GA – Y_4**		
	SS	dF	MS	F-Value	p-value
Model	3824.88	4	956.22	11.17	<0.0001
Residual	2140.25	25	85.61		
Lack of Fit	1722.24	20	86.11	1.03	0.5409
Pure Error	418.01	5	83.60		
Cor Total	5965.14	29			
R^2	0.6412				

Through the analysis of table 5, it is possible to see that the quartic regression model, used in the first three variables, presents a good fit for predicting the response, since the R^2 value is very close to 1. Regarding the fit presented by linear regression in the last parameter under study (GA EE (Y_4)), this reveals to be lower. Nonetheless, all the variables studied were considered for the model. As an example, the figure below (6) demonstrates the relationship

between the experimental values obtained and the predicted fit performed by the model for the four variables studied.

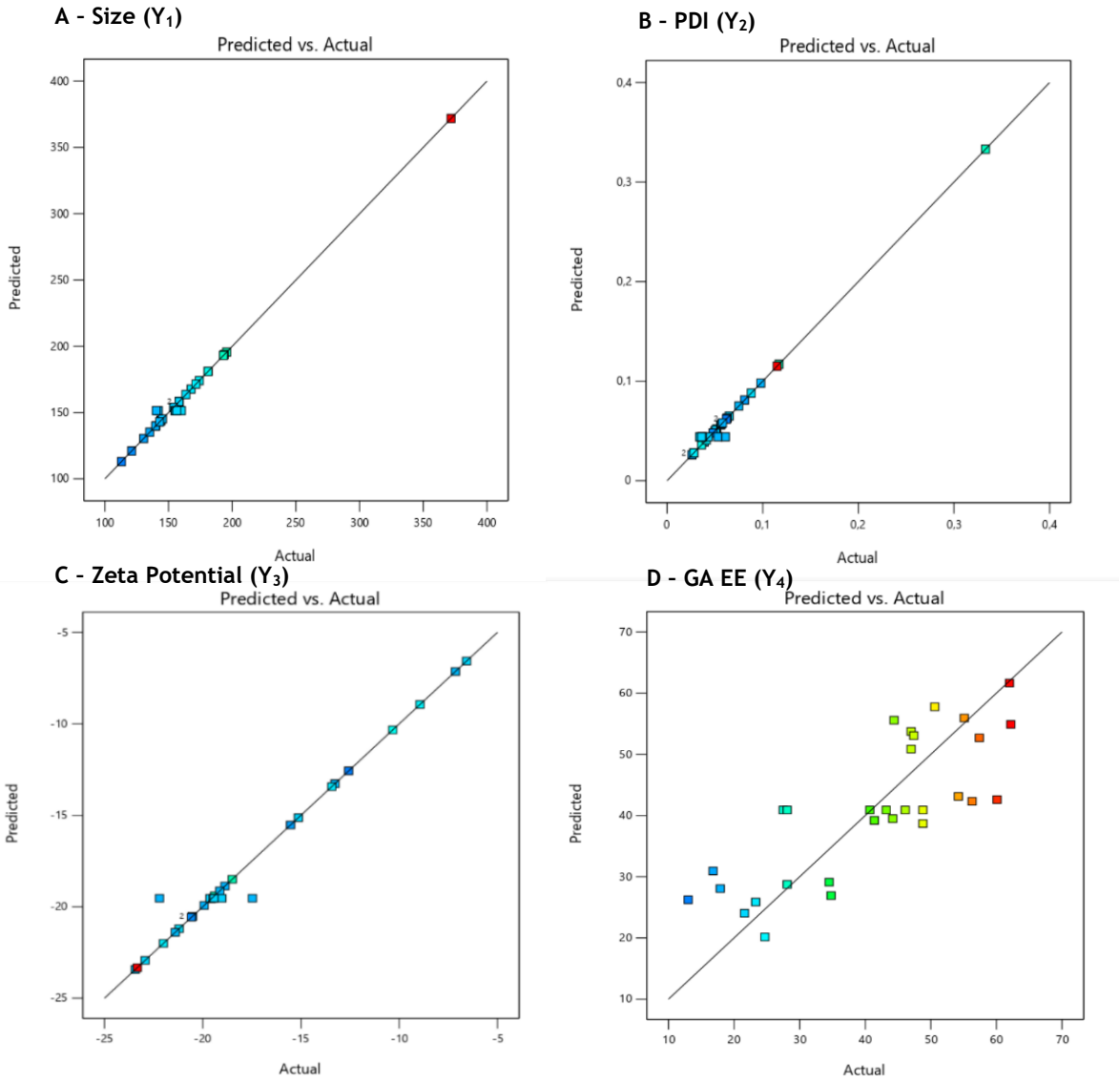


Figure 6 - Graphical plots between the experimental values obtained vs the predicted values for the significant variables, (A) Size (Y_1), (B) PDI (Y_2), (C) Zeta Potential (Y_3), and (D) GA EE (Y_4). The blue squares represent lower values, in contrast to red squares that represent higher values.

Through the analysis of figure 6, it is possible to notice the good fit performed for the first three variables, evidenced by the high values of R^2 (0.9941, 0.9935 and 0.9821, respectively) and a less good fit for the variable GA EE (Y_4), visually identified by a greater dispersion of the points to the fit line and a lower value of the coefficient of determination (0.6412).

In addition to the analysis mentioned above, the regression coefficient (RC) for all independent variables was also determined. The RC value of each variable and their joint interactions will be used in the equation of each studied response, reflecting the impact that

each of the independent variables has on the response under study. For this reason, the RC is represented with the positive or negative sign. In this way, when the value of the coefficient reveals to be positive, it means that the increase in that variable contributes positively to the increase in the value of the response. The table below (table 6) presents the RC and the p-value for each experimental variable, for each of the responses. Note that since the model used for the responses contains a high extent of terms, only the RC values corresponding to variables that were considered statistically significant ($p<0.05$) are presented in table 6. These values were also those considered for the representation of the equations obtained, present in A2.1 to A2.4, in Appendix A2.

Table 6 – RC and p-Value for all responses.

	Size – Y_1		**PDI – Y_2**	
	RC	**p-Value**	**RC**	**p-Value**
A – PLGA mass	-9.54	0.0523	-0.0792	<0.0001
B - % PVA	-74.93	<0.0001	-0.0055	0.3166
C–FA molecules/ NP	-1.75	0.6624	0.0003	0.9504
D–Sonication Cycles	-9.21	0.0581	0.0152	0.0276
AB	-7.26	0.0168	-0.0079	0.0323
BC	-8.21	0.0105		
BD	-7.73	0.0132		
A^2	11.24	0.0103	0.0696	<0.0001
B^2	43.66	<0.0001	0.0261	0.0009
A^2B	60.18	<0.0001		
AB^2	16.83	0.0112	0.0740	<0.0001
A^2B^2	-48.19	0.0004	-0.0937	<0.0001
	Zeta Potential – Y_3		**GA EE – Y_4**	
	RC	**p-Value**	**RC**	**p-Value**
A – PLGA mass	-0.5819	0.4423	1.44	0.4857
B - % PVA	1.44	0.0937	13.41	<0.0001
C– FA molecules/ NP	0.4752	0.5261	0.9149	0.6560
D–Sonication Cycles	0.9278	0.2410	1.10	0.5933
BC	-7.26	0.0009		
A^2B	-8.21	0.0023		
A^2B^2	-7.73	0.027		

In addition to the statistical values calculated by the software, it is also possible to analyse the impact that exist between the different independent variables for each of the responses in a visual way. Thus, through contour plots (2D) and surface plots (3D), the impact of each parameter on a given response under study is presented in the form of a color gradient. Figures 7, 8, 9 and 10 represent the contour and surface plots for the dependent variables size (Y_1), PDI (Y_2), zeta potential (Y_3) and GA EE (Y_4), respectively.

4.1.1. Effect on the NPs' Size

As already mentioned in subsection 2.4.1, particle size is crucial for the internalization process of the drug in the target tissue. Thus, particles with a size less than 200 nm are ideal for nano delivery since they can accumulate in the tumor tissue effectively due to the EPR effect [92]. After preparing all the desired nanoformulations by DoE, a size range of NPs between 113.0 nm (formulation 15) and 371.8 nm (formulation 19) was obtained. Figure 7 contains the contour and surface plots showing the effect of the independent variables on the obtained size of the NPs.

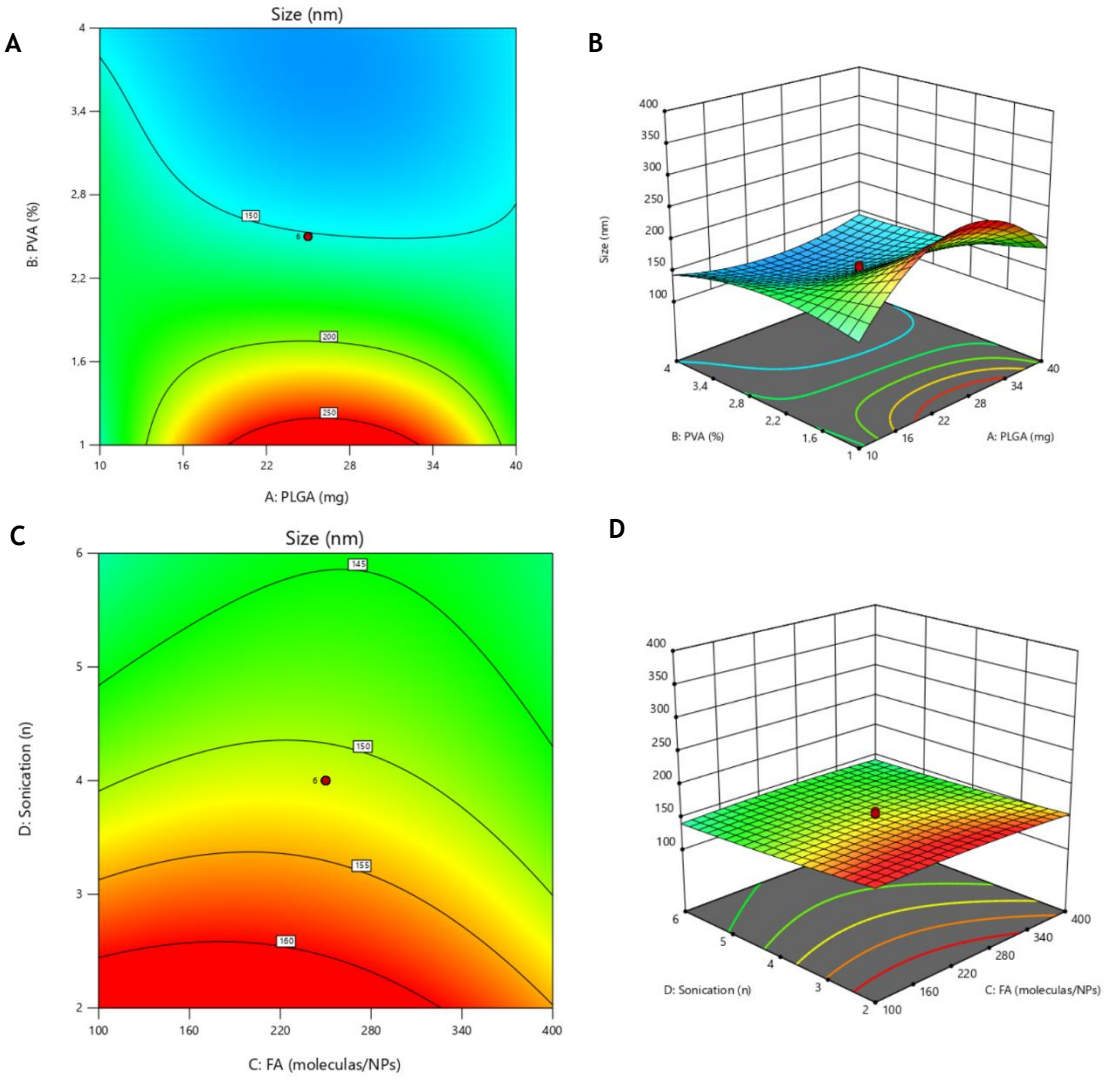


Figure 7 - (A)(B) Contour and (C)(D) surface plots of all independent variables on the NPs' size.

It is possible to notice, by the color gradient, that the colder tones (blue) represent values of lower sizes, in contrast to the warmer tones (red), which represent higher sizes. By observing images A and B, it is possible to see the effect of quantity of PLGA and the percentage of PVA

in NPs size. According to some authors, the amount of PLGA positively affects the size of the NPs since its increase reflects an increment in the viscosity of the organic phase and a consequent decrease in shear stress. Thus, the diffusion of this solvent into the aqueous phase is hindered, which causes the creation of emulsion droplets with larger dimensions [64]. However, in this work, the contrary effect was observed. Since, according to the value of RC and the obtained regression equation (eq. 1, Appendix A2), this variable has a negative effect on the size of NPs. In the work performed by Huang and Zhang, it was concluded that the size of NPs does not show a linear correlation with increasing polymer concentration [105]. It was found that this relationship was linear up to a certain concentration (20 mg/mL), and the size of the obtained nanoformulations was similar using 20 mg/mL or 40 mg/mL concentration. Thus, it can be stated that the size of the NPs is only predicted by the diffusion rate of the organic phase into the aqueous phase up to a certain concentration of the polymer [105]. By looking at the contour plot, it can be seen that the size of the NPs increases with increasing PLGA mass up to a certain value (approximately 35 mg) and after that the size starts to decrease, which is supported by the previously mentioned work.

Furthermore, the percentage of PVA negatively affected the NPs size, since this substance decreases the interfacial tension between the oiled droplets containing PLGA and the continuous aqueous phase, as verified through the RC value and equation obtained. This reveals that increasing the percentage of this variable results in formation of smaller NPs [106]. Another important factor to take into consideration is the sonication cycles, that showed a negative effect on the size of the nanoformulations, as verified through the RC value and plots. This happens because a longer sonication time/ more sonication cycles releases higher sonication energy, leading to rapid and uniform dispersion of the polymeric organic phase and lower polydispersity, culminating in a smaller size of the NPs [107].

4.1.2. Effect on NPs' PDI

Analogously to the analysis done previously for the size of the NPs, the PDI was also analyzed through the RC value and equation (eq. 2, Appendix A2) obtained, as well as the contour and surface plots represented in figure 8. PDI indicates the homogeneity of the sample, giving an indication of the different sizes of the NPs. Thus, the smaller the difference between the size of the NPs, the lower the PDI value will be, revealing, consequently, the monodispersity of the sample. Ideally, this value should be less than 0.1 for the sample to be considered monodisperse. Through the nanoformulations obtained, the range of PDI values varied between

0.026 (nanoformulation 12) and 0.333 (nanoformulation 17). Figure 8 contains the contour and surface plots obtained for the independent variables and their effect on the PDI of the NPs.

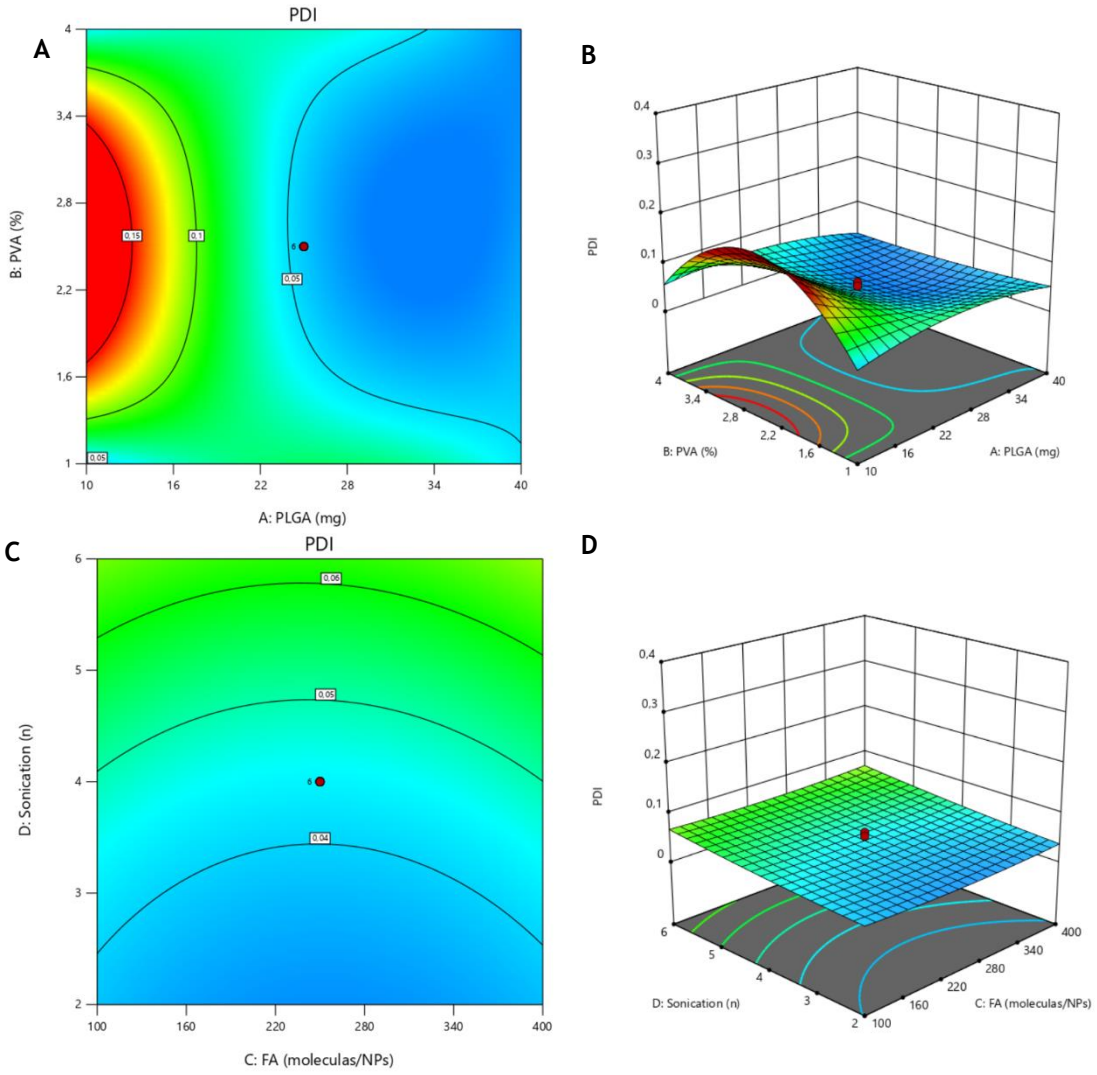


Figure 8 - (I)(III) Contour and (II)(IV) surface plots of all independent variables on the NPs' PDI.

By analyzing the RC value and the corresponding regression equation, the amount of PLGA and PVA negatively affect the PDI value obtained. A larger amount of polymer used in the formation of the nanoformulations can promote the formation of monodisperse samples, decreasing the PDI value obtained [108]. Furthermore, the decrease in the percentage of PVA can also influence the stability of the colloidal system, with a higher percentage showing greater stability leading to a more homogenous sample, reflecting in a lower PDI value [109]. Conversely, the number of FA molecules per NP and the number of sonication cycles positively affected this response. In addition, the greater the number of sonication cycles, the higher turbulence and pressure, leading to agglomeration and melting of the nanodrugs in the dispersed phase, which generates populations of various sizes, resulting in a higher value of PDI [110].

4.1.3. Effect on NPs' Zeta Potential

Another parameter under analysis was the zeta potential of the NPs, a characteristic that reveals the stability of the colloidal system. Through the nanoformulations produced along the experimental design, the zeta potential always maintained negative values due to the negative charge of the carboxyl group present in PLGA, presenting a range of values between -23.4 mV (nanoformulation 8) and -6.6 mV (nanoformulation 1). In this analysis the RC values, the corresponding equation (eq 3, Appendix A2) and the contour and surface plots, present in figure 9, were considered.

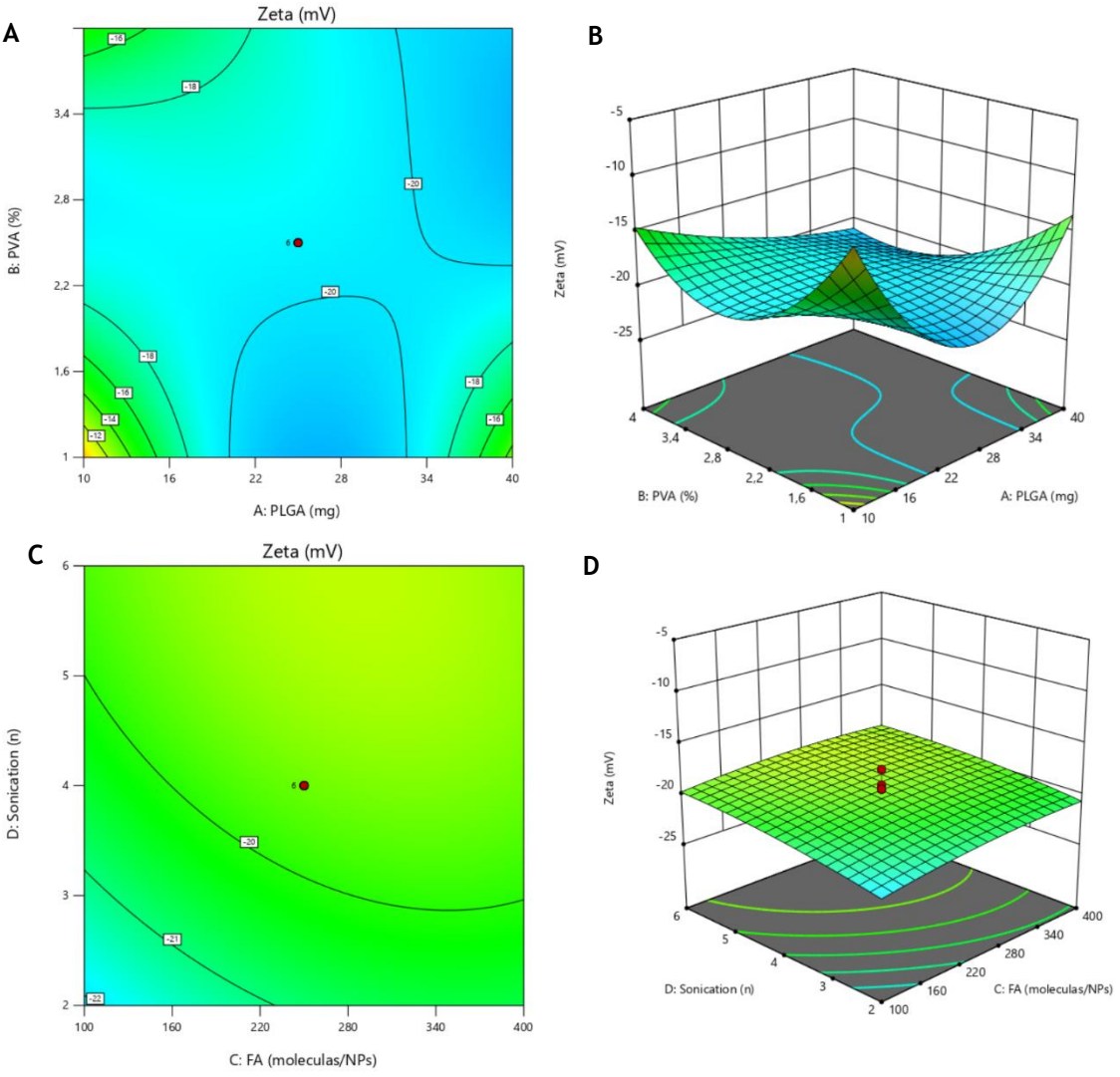


Figure 9 - (A)(C) Contour and (B)(D) surface plots of all independent variables on the NPs' Zeta Potential.

Through the analysis of the RC value and the corresponding regression equation, the amount of PLGA negatively affects the zeta potential value obtained, since this compound has a negatively charged carboxyl group, which translates into the negative value of this response [111]. On the contrary, the % of PVA, the number of FA molecules per NP and the number of sonication cycles affect positively this variable. Folic acid and PVA exhibit both neutral charge, and it is expected that with increasing number of FA molecules per NP, the absolute value of

the zeta potential would decrease, approaching neutrality. This can be explained by the fact that increasing the sonication time/number of sonication cycles results in smaller particles with better size distribution. Consequently, smaller particles have more surface area and higher negative charge as a result [112]. By analyzing the graphs, it is possible to see that they corroborate the conclusions from the previous statistical analysis.

4.1.4. Effect on GA EE

The encapsulation efficiency of the GA is a very important factor in the development of nanoformulations, as it is important to achieve the highest yield in the production of the NPs, to obtain a high percentage of drug successfully trapped in the nanoparticle. After preparation of the nanoformulations a range of GA EE was obtained between 13.0% (formulation 9) and 62.2% (formulation 15). Figure 10 shows the contour and surface plots obtained for the independent variables and what their influence is on EE.

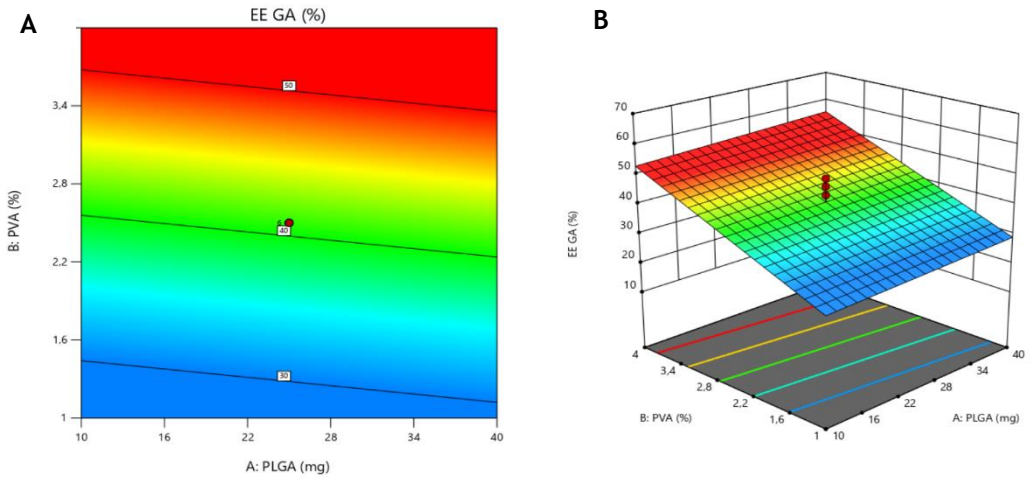


Figure 10 - (A) Contour and (B) surface plots of PLGA mass and % of PVA on the NPs' EE of GA.

According to the RC values and the regression equation (eq. 3, Appendix A2), all parameters positively affect the response variable. In other words, as the variables increase, the EE will also tend to increase. By observing the graphs and the RC value, it is possible to see that the amount of PVA is the most important factor in obtaining a higher EE, since for any value of the amount of PLGA, when the PVA increases, the EE also increases. The use of the optimal PVA concentration will affect the diffusion of the drug at the water/oil interface, with a higher concentration of the surfactant generally being reflected in a better diffusion of the drug, leading to an increase in EE [113]. Nevertheless, according to the equation obtained, the mass of PLGA used also reflects an increase in this response. According to the literature, the encapsulation efficiency generally increases with increasing relative amount of polymer matrices. This is because increasing the polymer concentration increases the viscosity of the organic phase. A higher viscosity of this phase provides greater resistance to mass transfer and

prevents diffusion of the drugs towards the outer aqueous phase, resulting in a higher %EE [114]. Also, a larger amount of PLGA is reflected in a larger matrix, thus obtaining more space to accommodate more GA molecules. The positive effect of the sonication cycles can be justified since increasing the sonication time is reflected in a faster evaporation of the oil phase, causing a faster hardening of the PLGA. Thus, the diffusion of the drug in the aqueous phase is lower, making it possible to obtain a higher EE [115]. Nevertheless, the graphs presented in figure 10 corroborate the conclusions drawn through the statistical analysis.

4.2 Protocol Optimization and Model Validation

After performing the analysis in the software and realizing which model was the best fit for each response, it was necessary to perform the optimization protocol, where the criteria for obtaining the optimal formulation were as follows. The independent variables were kept within the initial parameters. For the size of the NPs, a range of values between 140-200 nm was established (Y_1), the PDI value set to less than 0.09 (Y_2), the range of zeta potential values was maintained without any restriction, since all obtained nanoformulations were considered acceptable (Y_3), and the EE of GA was maximized up to 100% (Y_4). According to the mentioned parameters, the optimal values of the independent variables predicted by the software are shown in table 7.

Table 7 - Optimal formulation prediction for GA loaded PLGA NPs.

Parameter	Independent variable	Units	Optimal Value
A	PLGA mass	mg	40
B	PVA	%	4
C	FA molecules/NP	#	398
D	Sonication Cycles	#	4

To validate the model and the predicted protocol, five nanoformulations with the optimal characteristics were produced and their mean and standard deviation were calculated. Table 8 presents the comparison between the optimal responses predicted by the model and the experimental results obtained.

Table 8 - Predicted *versus* experimental values. The experimental results are represented as mean ± SD (n=5).

	Predicted Values	Experimental Values
Size (nm)	140 (123-157)	153 ± 9 (142-163)
PDI	0.05 (0.02-0.07)	0.05 ± 0.01 (0.03-0.06)

Zeta Potential (mV)	-21.9 (-32.7-[-18.9])	-27 ± 2 (-25.4-[-29.5])
GA EE (%)	56.3 (48.3-64.4)	50.8 ± 3.9 (46.3-54.6)

By analyzing the table, it is possible to notice that the average responses of the prepared nanoformulations are within the range predicted by the software, revealing a good prediction and mathematical adjustment of the model. Thus, the optimal nanoformulations produced presented ideal characteristics for possible administration, namely: a size less than 200 nm that facilitates the internalization of the drug in the target tissue and greater than 100 nm, which reduces the possibility of eventual absorption by the body; PDI less than 0.1, indicating the monodispersity of the sample; negative zeta potential due to the carboxyl group present in the PLGA composition and the neutrality of the FA, with high absolute values, suggesting the stability of the colloidal system. Furthermore, the EE value obtained proved to be reasonable, translating to approximately half the mass of the drug being trapped inside the NPs.

4.3 FTIR Analysis

FTIR analysis allows understanding through its spectra which structural details exist in a particle since they represent a unique chemical bond for each molecule [116]. FTIR analysis was used to confirm the correct preparation of conjugation of GA-loaded PLGA NPs with FA. PLGA can be divided into 5 main regions. At 3450-3500 cm^{-1} peak corresponding to OH end group; 2885-3010 cm^{-1} corresponding to C-O stretching; around 1762.6 cm^{-1} due to C=O stretching; between 1450-850 cm^{-1} due to C-H bends, and finally, at 1186-1089 cm^{-1} the C-O stretching peak is represented [117]. As for GA, this compound presents in the FTIR spectrum small bands corresponding to the O-H hydrogen bonds between 3060 cm^{-1} and 3491 cm^{-1}. The C=O group also appears represented through the bands 1307 cm^{-1} and 1605 $cm^{-1}$and also a vibrational band at 1021 cm^{-1} corresponding to the vibration of the benzene ring [118].For the FA absorption spectrum, it is possible to find the following: 3100-3500 cm^{-1} corresponding to OH carboxylic of glutamic acid moiety and NH group of pterin ring stretching; 1693 cm^{-1} corresponding to C=O carboxylic group; 1604-1605 cm^{-1} for N-H bending; and 1485-1519 cm^{-1} corresponding to phenyl and pterin ring. There are also other peaks like: 2362 cm^{-1} that is attributed to the N^{+}-H stretching vibration band of C=N^{+}-H - on the PT ring, 1650 cm^{-1} for C=O amide; 1639 cm^{-1} corresponding to C=N, and 1619 cm^{-1} related to C=C aromatic [119], [120]. Below, in figure 11, the FTIR spectrum of the GA-PLGA NPs without any functionalization process and the FA stock solution for the conjugation of the NPs are represented.

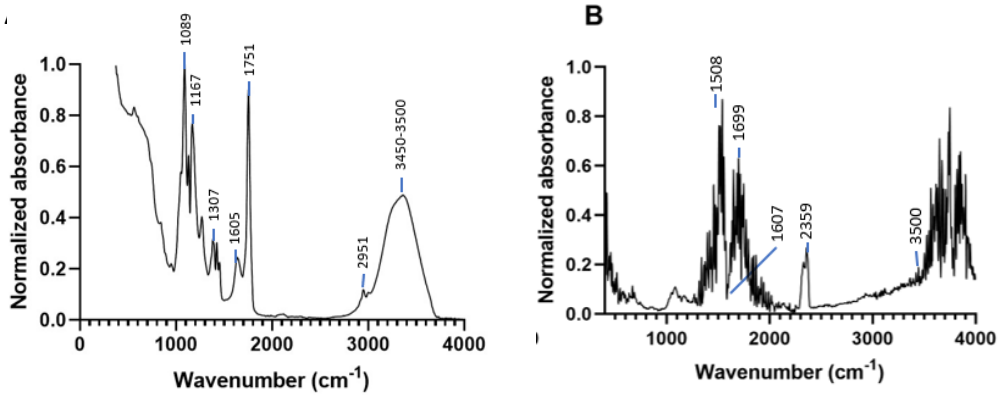


Figure 11 - FTIR absorbance spectra of (A) GA-PLGA NPs and (B) Stock FA.

Analyzing the figure above it is possible to observe the main characteristic peaks/regions of the PLGA, GA, and FA identified in the literature are also observed in the recorded spectra.

To study whether the FA conjugation process was successful, the FTIR spectra of the FA-GA-loaded PLGA NPs were also recorded. Figure 12 shows the FTIR spectrum of GA-PLGA NPs after conjugation with FA together with the spectrum of PLGA NPs before functionalization and the FA stock spectrum.

As shown in figure 12, after conjugation with FA, it is possible to see that the FA-GA-PLGA NPs present characteristic peaks of this compound, namely: 1508 cm^{-1}, 1652 cm^{-1} zone, and 2359 cm^{-1}, thus revealing the success of this functionalization.

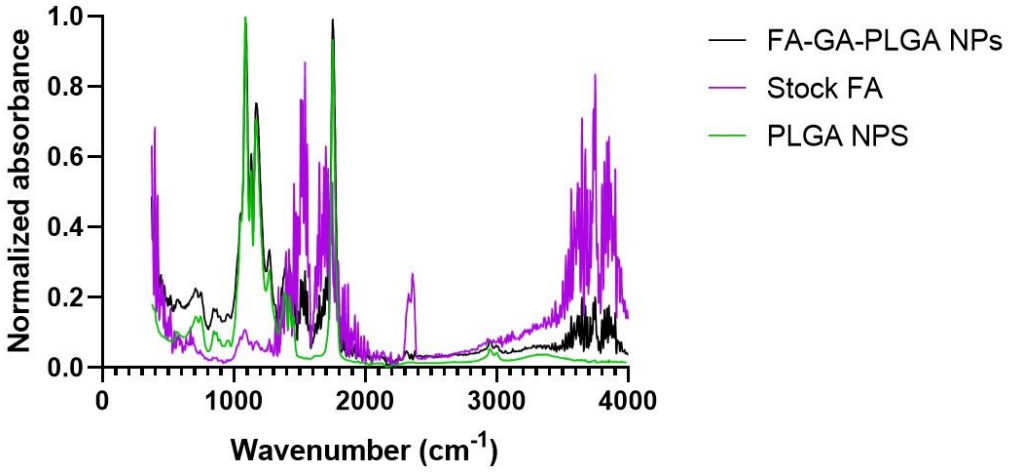


Figure 12 - FTIR absorbance spectrum of FA-GA-PLGA NPs, PLGA NPs, and FA stock solution.

4.4 TEM Analysis

Through TEM analysis it was possible to confirm the shape and dimensions corresponding to the FA-GA-loaded NPs that were produced. Figure 13 reveals the result obtained after performing this technique, where, from the observation of the same it is possible to realize that the NPs present a spherical and regular shape, as expected for polymeric NPs. In addition, it is possible to observe a darker line around the NPs corresponding to their coating, due to the use of PVA. Finally, it is important mentioning that the size shown is smaller than the one determined through the DLS technique, since the DLS shows the hydrodynamic size of the NPs, constituted by the nanoparticle-electron ion layer assembly that surrounds it [121].

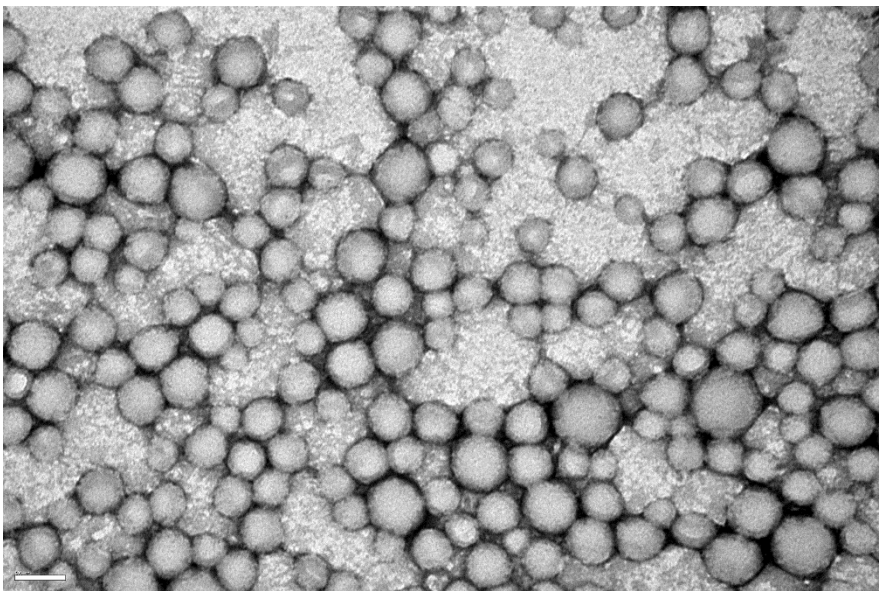


Figure 13 - Morphological characterization of FA-GA-loaded PLGA NPs by TEM.

4.5 Release Profile of GA

The release profile of the drug encapsulated in the nanoformulations was evaluated over time by mimicking physiological conditions (37º C in PBS, 0.01 M) for two different pHs, 6.4 and 7.4. This *in vitro* profile is an important aspect to consider since it provides essential information about the ability to modify drug release. Thus, it is an important parameter in the evaluation of its safety and efficacy and can be correlated with *in vivo* behavior [122].

The drug release profile is dependent on a few factors, namely: solubility, drug diffusion, diffusion agent, and encapsulation methods [123]. Figure 14 shows the release profiles of GA under physiological conditions at pH 7.4 and 6.4, respectively.

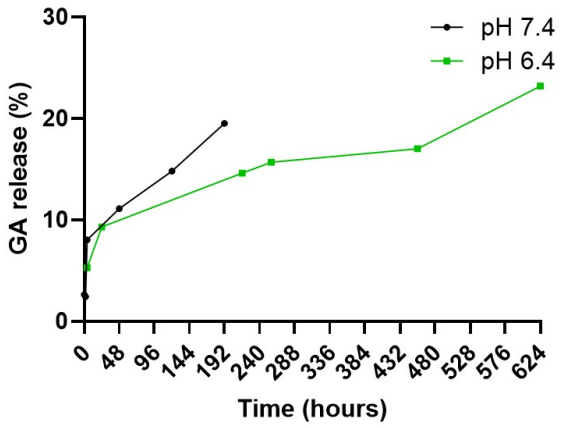


Figure 14 - Release profile of FA-GA-loaded PLGA NPs overtime for pH=7.4 and 6.4.

By analyzing figure 14, it is possible to see that the drug release profile in NPs for pH 7.4 conditions reveals an increasing character over 192 hours. A biphasic pattern emerges in this release, with an initial release (in the first 4 hours) of 8%, followed by a slower and controlled release over the following days, reaching a release of 20% after 8 days (192 hours). Regarding the release profile of GA under physiological conditions at pH 6.4, a faster initial release was also observed after 4 hours (5%), followed by a slower release over the remaining days, reaching a 23% drug release percentage after 26 days (624 hours), also revealing a biphasic profile. In general, there is always an initial burst release caused by de-adsorption of the compounds adsorbed to the NPs' surface [124]. After this initial phase, three forms of drug release arise, namely: drug diffusion from the matrix of the PLGA NPs, erosion of the NPs, and hydrolysis [125]. Furthermore, it is important to note that PLGA is useful for controlled release because it degrades over several weeks by hydrolysis forming by-products that are easily metabolized by the body [126]. Finally, it should be noted that the amount of GA that was released in both physiological conditions over time was not as desired, given the percentages obtained. Despite its slow and controlled release, ideally the amount of drug released should have been greater.

4.6 NPs' Stability in Storage Conditions

To evaluate the colloidal stability of the nanoformulations under storage conditions, the physicochemical properties of the optimal NPs were measured over 6 weeks. Thus, the 5 batchs (FA-GA-loaded PLGA NPs) were stored in storage conditions where, their stability was measured using the DLS technique once a week. The results obtained are presented in table 9, showing the mean size (nm), PDI and zeta potential (mV) obtained and their SD.

Table 9 - Optimal FA-GA-loaded PLGA NPs stability in storage conditions over 8 weeks (mean±SD, n=5).

Time (weeks)	Mean size (nm)	PDI	Zeta potential (mV)
pH 7.0			
0	153 ± 9	0.05 ± 0.01	- 27 ± 2
1	153 ± 9	0.03 ± 0.01	- 22 ± 3
2	150 ± 9	0.040 ± 0.005	- 21 ± 2
3	152 ± 9	0.06 ± 0.03	- 21 ± 2
4	150 ± 8	0.04 ± 0.01	- 22 ± 1
5	152 ± 7	0.04 ± 0.01	- 22 ± 1
6	151 ± 8	0.05 ± 0.01	- 21 ± 2
7	152 ± 8	0.04 ± 0.02	- 23 ± 2
8	149 ± 9	0.04 ± 0.01	- 20 ± 2

Through the analysis of the results, it can be inferred that over time the size (nm) and PDI of the NPs did not change significantly, since no statistically significant changes were observed in these properties ($p>0.05$), revealing stability in these two parameters. Regarding the zeta potential (mV), the decrease in its value was significant ($p<0.05$), however this change does not show instability of the NPs under storage conditions, since this decrease may occur by successively applying an electric potential in the sample.

4.7 NPs' Stability in Physiological Conditions

The colloidal stability of the nanoformulations under physiological conditions was also evaluated. The size (nm), PDI and zeta potential (mV) of FA-GA-loaded PLGA NPs were measured over several weeks in simulated physiological conditions (PBS 0.01 M, pH 6.4) and (PBS 0.01 M, pH 7.4). The results obtained are summarized in table 10, present below.

Table 10 - Optimal FA-GA-loaded PLGA NPs stability in physiological conditions over 3 weeks at.

Time (hours)	Mean size (nm)	PDI	Zeta potential (mV)
PBS 0.01 M, pH 6.4			
4	134	0.06	-1.2
24	134	0.03	-2.6
120	133	0.03	-0.9
216	146	0.08	-3.8
288	143	0.02	-4.3
456	134	0.05	-2.4
624	150	0.08	-4.0
PBS 0.01 M, pH 7.4			
0	143	0.03	-1.4
2	140	0.04	-1.4

4	144	0.03	-1.0
24	144	0.02	-1.4
48	148	0.03	-2.5
120	141	0.06	-0.9
192	129	0.09	-3.0
288	139	0.03	-4.3
360	139	0.06	-1.8

The FA-GA-loaded PLGA NPs stored in simulated physiological conditions were stable over 3 weeks, for both studied pHs. Through the results it is possible to realize that for pH 7.4: the largest size variation was 19 nm (size decreased from 148 nm at 48 hours to 129 nm at 192 hours), however, the remaining measured sizes are all in the range of 139 to 144 nm, a variation of only approximately 5 nm. Over time the PDI showed some increase, however it always proved to be optimal, i.e., below 0.1. Regarding the results obtained for pH 6.4: the largest size variation was 17 nm, with the size increasing from 133 nm to 150 nm between 120h and 624h, the other sizes being quite close. The PDI, as before, showed values less than 0.1, proving the homogeneity and monodispersity of the sample over time. The zeta potential was always quite close to neutral, showing its farthest value after 288 hours (-4.3 mV) for both pHs. As expected, under physiological conditions, since the NPs were suspended in PBS, the zeta potential obtained is very close to neutral by the charge neutralization effect [127]. When the NPs are resuspended in PBS (buffer solution that helps to maintain a constant pH), the zeta potential tends to approach neutrality. This is due to the free charges in the PBS interacting with the chemical groups on the surface of the NPs, masking the negative sign of the NPs [128]. However, it is possible to state that the stability of the NPs produced is maintained since this is promoted by the steric stabilization of the PVA and also by the surface charges. This biocompatible polymer promotes the monodispersity of the samples and their stabilization through its adsorption on the surface, thus avoiding the agglomeration of the nanoformulations [129].

4.8 NPs' Antiproliferative Activity

As mentioned in the methodology section regarding cell cultures (3.11 and 3.12), two human cell lines, U251 referring to GBM and NHA referring to healthy brain cells, were used to evaluate the antiproliferative activity of FA-GA-loaded PLGA NPs in *in vitro* conditions. To compare the antiproliferative effect of free GA and GA encapsulated in FA-PLGA NPs, increasing concentrations of free drug and FA-GA-loaded-PLGA NPs were tested. Figure 15 shows the survival inhibition curves for each of the cell lines for both forms of administered natural compound.

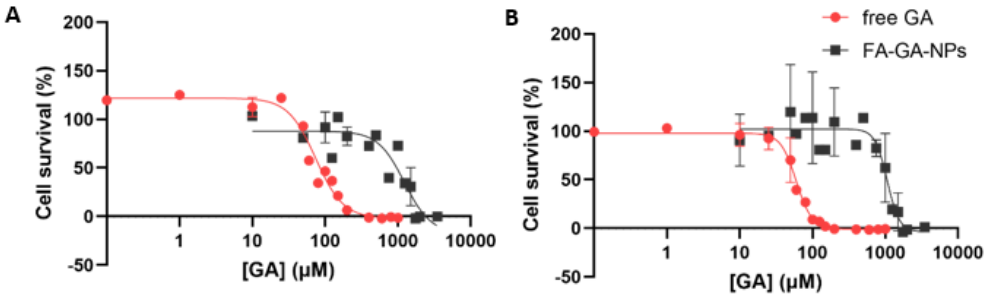


Figure 15 - Cell survival curve after 72-hour treatment with free GA and FA-GA-NPs for (A) NHA cell line (B) U251 cell line.

Through the results obtained it is possible to see that cell survival in both cell lines under study present a decrease with increasing GA concentration. The cell survival profile for free GA presents a well-defined curve for both cell lines, with the survival rate being practically null starting at 200 μM of GA. Regarding the antiproliferative ability of FA-GA-loaded NPs in both cell lines, it is possible to see that a much higher concentration of drug is required to obtain the same result of inhibition of cell survival caused by free GA.

The half-maximal inhibitory concentration (IC_{50}) is a determining factor to consider in cell tests, since it is representative of the amount of drug that is required to inhibit the biological process, in this case cell survival, by half [130]. IC_{50} values were obtained from the cell survival plots and are shown in table 11 below.

Table 11 - IC_{50} after 72 hours using free GA and FA-GA-NPs for both cell lines.

	IC_{50} (μM)	
	Free GA	**FA-GA-NPs**
U251	60 ± 10	1073 ± 231
NHA	87 ± 7	1099 ± 466

Comparing the obtained IC_{50} values, it can be concluded that free GA therapy inhibited cell proliferation more efficiently when compared to NPs therapy. Thus, the IC_{50} values for the free compound were lower since much higher concentrations of NPs are required to obtain the same therapeutic effect. This can be explained by the slow release of GA, resulting in an inability to produce the same intensity of antiproliferative activity that the free drug is capable of [42]. Through the release results presented in section 4.5, it is possible to see that after 72 hours, only approximately 12% of GA was released from the NPs. Considering that the cell experiments were performed in this period, it is expected that there is a reduced amount of GA in contact with the cells, which reveals that the total concentration of GA is not available during this time, resulting in a lower antiproliferative capacity of the NPs. However, it is expected that

the GA encapsulation in FA-PLGA NPs will be able to improve its efficacy *in vivo*, by increasing GA accumulation by directing the NPs to the tumor brain tissue overexpressing FA receptors.

It is also important to mention that since GA is a natural compound with antioxidant properties, the NHA cell line was used to compare the survival rate of these cells with a cancer cell line. According to the literature, it would be expected that the survival rate of the NHA line would be higher compared to U251, for the same concentration of drug used [131]. The results obtained show that the difference between the effect of free GA on the two lines is significant, demonstrating that indeed the natural compound has more antiproliferative effect on the tumor line than on the healthy line. Regarding the difference in the effect of NPs between the two cell lines, this proved to be non-significant, as evidenced by the close IC_{50} values presented.

Finally, the biocompatibility of FA-PLGA NPs without GA was also evaluated, in order to prove that the NPs are safe for administration, and that the antiproliferative effect comes from the continuous release of GA and not from the PLGA NPs. Figure 16 presents the results of the biocompatibility tests of the FA-PLGA NPs obtained for both cell lines.

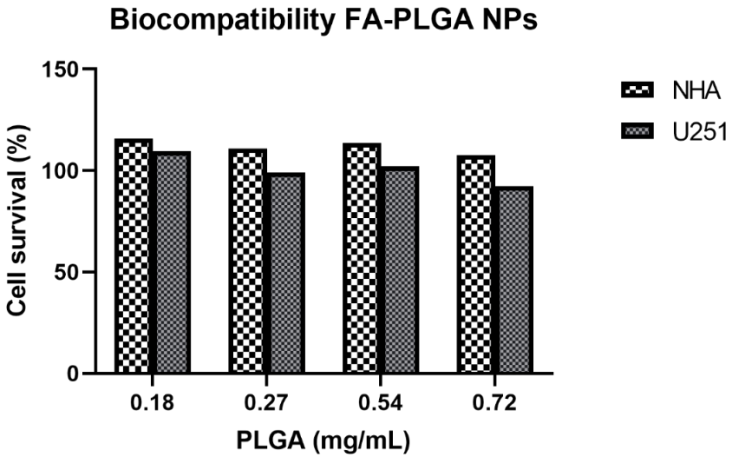


Figure 16 - Cell survival rate of FA-PLGA NPs for U251 and NHA cell lines.

From the results, it can be concluded that the NPs are biocompatible as they do not cause toxicity in the tested range of concentrations, thus indicating that the effect that is observed in FA-GA-loaded PLGA NPs is due to the use of GA, and not due to PLGA NPs. A concentration range of PLGA NPs between 0.18-0.72 mg/mL was chosen for this assay. These were chosen to match the concentration range of 500-2000 μM of GA, which represents the concentrations at which cell survival began to decrease for the NPs in both cell lines.

Chapter 5

Conclusions and Future Perspectives

Cancer has been, in the last decades, a disease that affects a huge number of people all over the world and for which treatment solutions are continuously being tried. One of the deadliest types of cancer is GBM. In this sense, nanomedicine has emerged as a major weapon in the fight against this disease, both in its diagnosis and treatment.

The therapeutic properties of natural compounds have been the subject of constant studies, due to their antioxidant and anti-carcinogenic properties. GA is one of these compounds that has interesting properties for fighting GBM. Nevertheless, due to its low solubility, it is necessary to resort to nanomedicine, namely the production of NPs, to make the use of this natural compound a viable solution.

The main objective of this work was, therefore, to use PLGA NPs to effectively encapsulate this drug. In addition, the surface of this nanosystem was successfully conjugated with FA. It is also important that this nanoformulation has a set of characteristics - such as size, PDI, zeta potential, and EE - ideal for its effective internalization in the tumor tissue, without compromising the cell viability of normal cells. In this way, the DoE was used to understand the impact of the variables used in the production of nanformulations. Thus, a central composite design was implemented to optimize the nanosystem, through which 30 formulations were produced, subsequently creating a mathematical model correlating the independent variables with the responses to be studied (size, PDI, zeta potential, and EE). Finally, an optimal model was obtained, predicted by the software: 40 mg PLGA, 4% PVA, 398 molecules of FA/ NP, and 4 sonication cycles. The optimal formulation was then produced, meeting the software predictions, verifying NPs with size less than 200 nm, PDI less than 0.01, negative zeta potential, and EE% close to 50%.

In addition, the drug was released over 15 days for different characteristics of the physiological medium (pH 6.4 and pH 7.4). The results obtained showed a slow and controlled release of GA, however a low percentage of released compound (approximately 20%) was achieved. The stability of the optimal NPs under storage and physiological conditions was also evaluated, and in both cases the physicochemical properties of the nanoformulations remained stable.

The antiproliferative effect of the NPs was studied, and compared with free GA, in the two cell lines U251 and NHA, through *in vitro* studies. For the free GA and the FA-GA-loaded PLGA NPs, it was confirmed that the cell survival rate shows a decrease with increasing drug concentration. However, free GA therapy inhibited cell proliferation more efficiently when compared to FA-GA NPs therapy. These results can be explained due to the slow release of GA over time, as verified in release tests. Furthermore, the difference between the effect of free GA in the two lines was shown to be significant, revealing that GA exhibits greater antiproliferative effect in the tumor line than in the healthy line. Further toxicity tests with control unloaded FA-NPs also allowed proving that the FA-PLGA NPs are biocompatible and that the observed antiproliferative effect of NPs comes from the continuous release of GA.

As future perspectives, it will be necessary to extend the work performed so far in order to evaluate the efficacy of the nanosystem. In this sense, it is important to evaluate the cytotoxicity of the produced NPs and the free drug in more GBM cell lines. Pharmokinetics and biodistribution studies using in vivo animal models may also be a test option.

References

[1] K. Urbanska, J. Sokolowska, M. Szmidt, and P. Sysa, “Glioblastoma multiforme - An overview,” *Wspolczesna Onkologia*, vol. 18, no. 5. Termedia Publishing House Ltd., pp. 307–312, 2014. doi: 10.5114/wo.2014.40559.

[2] L. Jena, E. McErlean, and H. McCarthy, “Delivery across the blood-brain barrier: nanomedicine for glioblastoma multiforme,” *Drug Delivery and Translational Research*, vol. 10, no. 2. Springer, pp. 304–318, Apr. 01, 2020. doi: 10.1007/s13346-019-00679-2.

[3] S. T. Shah *et al.*, “Surface functionalization of iron oxide nanoparticles with gallic acid as potential antioxidant and antimicrobial agents,” *Nanomaterials*, vol. 7, no. 10, Oct. 2017, doi: 10.3390/nano7100306.

[4] A. Hassani, M. M. S. Azarian, W. N. Ibrahim, and S. A. Hussain, “Preparation, characterization and therapeutic properties of gum arabic-stabilized gallic acid nanoparticles,” *Sci Rep*, vol. 10, no. 1, Dec. 2020, doi: 10.1038/s41598-020-71175-8.

[5] A. Narmani *et al.*, “Folic acid functionalized nanoparticles as pharmaceutical carriers in drug delivery systems,” *Drug Dev Res*, vol. 80, no. 4, pp. 404–424, Jun. 2019, doi: 10.1002/ddr.21545.

[6] National Cancer Institute, “The Cancer Genome Atlas - Glioblastoma Multiforme Study - NCI.” https://www.cancer.gov/about-nci/organization/ccg/research/structural-genomics/tcga/studied-cancers/glioblastoma (accessed Nov. 20, 2022).

[7] F. Hanif, K. Muzaffar, K. Perveen, S. M. Malhi, and S. U. Simjee, “Glioblastoma multiforme: A review of its epidemiology and pathogenesis through clinical presentation and treatment,” *Asian Pacific Journal of Cancer Prevention*, vol. 18, no. 1. Asian Pacific Organization for Cancer Prevention, pp. 3–9, 2017. doi: 10.22034/APJCP.2017.18.1.3.

[8] C. Alifieris and D. T. Trafalis, “Glioblastoma multiforme: Pathogenesis and treatment,” *Pharmacology and Therapeutics*, vol. 152. Elsevier Inc., pp. 63–82, Jun. 29, 2015. doi: 10.1016/j.pharmthera.2015.05.005.

[9] H. Ohgaki and P. Kleihues, “The definition of primary and secondary glioblastoma,” *Clinical Cancer Research*, vol. 19, no. 4. pp. 764–772, Feb. 15, 2013. doi: 10.1158/1078-0432.CCR-12-3002.

[10] I. Z. Renault and D. Golgher, “Molecular Genetics of Glioblastomas. Defining Subtypes and Understanding the Biology,” *Neuroimaging Clinics of North America*, vol. 25, no. 1. W.B. Saunders, pp. 97–103, 2015. doi: 10.1016/j.nic.2014.09.007.

[11] X. Zhang, W. Zhang, W. D. Cao, G. Cheng, and Y. Q. Zhang, “Glioblastoma multiforme: Molecular characterization and current treatment strategy (Review),” *Experimental and Therapeutic Medicine*, vol. 3, no. 1. pp. 9–14, Jan. 2012. doi: 10.3892/etm.2011.367.

[12] X. Guan *et al.*, “Molecular subtypes of glioblastoma are relevant to lower grade glioma,” *PLoS One*, vol. 9, no. 3, Mar. 2014, doi: 10.1371/journal.pone.0091216.

[13] K. Tomczak, P. Czerwińska, and M. Wiznerowicz, “The Cancer Genome Atlas (TCGA): An immeasurable source of knowledge,” *Wspolczesna Onkologia*, vol. 1A. Termedia Publishing House Ltd., pp. A68–A77, 2015. doi: 10.5114/wo.2014.47136.

[14] R. Batash, N. Asna, P. Schaffer, N. Francis, and M. Schaffer, “Glioblastoma Multiforme, Diagnosis and Treatment; Recent Literature Review,” *Curr Med Chem*, vol. 24, no. 27, May 2017, doi: 10.2174/0929867324666170516123206.

[15] Gliocure, “Glioblastoma : Gliocure,” 2017. https://www.gliocure.com/en/patients/glioblastoma/ (accessed Nov. 20, 2022).

[16] National Brain Tumor Society, “About Glioblastoma,” 2022. https://braintumor.org/events/glioblastoma-awareness-day/about-glioblastoma/ (accessed Nov. 20, 2022).

[17] M. Korja *et al.*, “Glioblastoma survival is improving despite increasing incidence rates: A nationwide study between 2000 and 2013 in Finland,” *Neuro Oncol*, vol. 21, no. 3, pp. 370–379, Feb. 2019, doi: 10.1093/neuonc/noy164.

[18] W. Wu *et al.*, “Glioblastoma multiforme (GBM): An overview of current therapies and mechanisms of resistance,” *Pharmacological Research*, vol. 171. Academic Press, Sep. 01, 2021. doi: 10.1016/j.phrs.2021.105780.

[19] B. M. Alexander and T. F. Cloughesy, “JOURNAL OF CLINICAL ONCOLOGY Adult Glioblastoma,” *J Clin Oncol*, vol. 35, pp. 2402–2409, 2017, doi: 10.1200/JCO.2017.

[20] A. F. Tamimi and M. Juweid, *Glioblastoma*. Codon Publications, 2017. doi: 10.15586/codon.glioblastoma.2017.

[21] O. G. Taylor, J. S. Brzozowski, and K. A. Skelding, “Glioblastoma multiforme: An overview of emerging therapeutic targets,” *Frontiers in Oncology*, vol. 9, no. SEP. Frontiers Media S.A., Sep. 01, 2019. doi: 10.3389/fonc.2019.00963.

[22] O. Stringfield *et al.*, “Multiparameter mri predictors of long-term survival in glioblastoma multiforme,” *Tomography*, vol. 5, no. 1, pp. 135–144, Mar. 2019, doi: 10.18383/j.tom.2018.00052.

[23] K. Anjum *et al.*, “Current status and future therapeutic perspectives of glioblastoma multiforme (GBM) therapy: A review,” *Biomedicine and Pharmacotherapy*, vol. 92. Elsevier Masson SAS, pp. 681–689, Aug. 01, 2017. doi: 10.1016/j.biopha.2017.05.125.

[24] C. von Neubeck, A. Seidlitz, H. H. Kitzler, B. Beuthien-Baumann, and M. Krause, “Glioblastoma Multiforme: Emerging treatments and stratification markers beyond new drugs,” 2015.

[25] Y. J. R. P. et al. Gaillard F, “Stupp protocol for glioblastoma,” *Radiopaedia.org*.

[26] M. Huang, J. J. Lu, and J. Ding, “Natural Products in Cancer Therapy: Past, Present and Future,” *Natural Products and Bioprospecting*, vol. 11, no. 1. Springer, pp. 5–13, Feb. 01, 2021. doi: 10.1007/s13659-020-00293-7.

[27] S. J. Huh, W. Park, and D. H. Choi, “Recent trends in intensity-modulated radiation therapy use in Korea,” *Radiat Oncol J*, vol. 37, no. 4, pp. 249–253, Dec. 2019, doi: 10.3857/roj.2019.00577.

[28] M. A. Dymova, S. Y. Taskaev, V. A. Richter, and E. V. Kuligina, “Boron neutron capture therapy: Current status and future perspectives,” *Cancer Communications*, vol. 40, no. 9. John Wiley and Sons Inc, pp. 406–421, Sep. 01, 2020. doi: 10.1002/cac2.12089.

[29] S. Mallick, R. Benson, A. Hakim, and G. K. Rath, “Management of glioblastoma after recurrence: A changing paradigm,” *Journal of the Egyptian National Cancer Institute*, vol. 28, no. 4. National Cancer Institute, Cairo University, pp. 199–210, Dec. 01, 2016. doi: 10.1016/j.jnci.2016.07.001.

[30] J. F. Hsu *et al.*, “Nanotechnology and nanocarrier-based drug delivery as the potential therapeutic strategy for glioblastoma multiforme: An update,” *Cancers*, vol. 13, no. 2. MDPI AG, pp. 1–22, Jan. 02, 2021. doi: 10.3390/cancers13020195.

[31] S. Nagpal, “The Role of BCNU Polymer Wafers (Gliadel) in the Treatment of Malignant Glioma,” *Neurosurgery Clinics of North America*, vol. 23, no. 2. pp. 289–295, Apr. 2012. doi: 10.1016/j.nec.2012.01.004.

[32] K. Zhai, M. Siddiqui, B. Abdellatif, A. Liskova, P. Kubatka, and D. Büsselberg, “Natural compounds in glioblastoma therapy: Preclinical insights, mechanistic pathways, and outlook,” *Cancers*, vol. 13, no. 10. MDPI, May 02, 2021. doi: 10.3390/cancers13102317.

[33] M. Kundu, S. Das, D. Dhara, and M. Mandal, “Prospect of natural products in glioma: A novel avenue in glioma management,” *Phytotherapy Research*, vol. 33, no. 10. John Wiley and Sons Ltd, pp. 2571–2584, Oct. 01, 2019. doi: 10.1002/ptr.6426.

[34] V. Desai and A. Bhushan, “Natural Bioactive Compounds: Alternative Approach to the Treatment of Glioblastoma Multiforme,” *BioMed Research International*, vol. 2017. Hindawi Limited, 2017. doi: 10.1155/2017/9363040.

[35] K.-S. Park, S.-Y. Yoon, S.-H. Park, and J.-H. Hwang, “Anti-Migration and Anti-Invasion Effects of Curcumin via Suppression of Fascin Expression in Glioblastoma Cells,” *Brain Tumor Res Treat*, vol. 7, no. 1, p. 16, 2019, doi: 10.14791/btrt.2019.7.e28.

[36] M. N. Manjunath C, “In vitro cytotoxicity of cardamom oil, lemon oil, and jasmine oil on human skin, gastric, and brain cancer cell line,” *J Cancer Res Ther* .

[37] P. Zou, X. Liu, G. Li, and Y. Wang, “Resveratrol pretreatment attenuates traumatic brain injury in rats by suppressing NLRP3 inflammasome activation via SIRT1,” *Mol Med Rep*, vol. 17, no. 2, pp. 3212–3217, Feb. 2018, doi: 10.3892/mmr.2017.8241.

[38] A. Faried *et al.*, “Anticancer effects of gallic acid isolated from Indonesianherbal medicine, Phaleria macrocarpa(Scheff.)Boerl, on human cancer cell lines,” 2006.

[39] Y. Jiang, J. Pei, Y. Zheng, Y. jing Miao, B. zhong Duan, and L. fang Huang, “Gallic Acid: A Potential Anti-Cancer Agent,” *Chinese Journal of Integrative Medicine*, vol. 28, no. 7. Springer Science and Business Media Deutschland GmbH, pp. 661–671, Jul. 01, 2022. doi: 10.1007/s11655-021-3345-2.

[40] S. Verma, A. Singh, and A. Mishra, “Gallic acid: Molecular rival of cancer,” *Environ Toxicol Pharmacol*, vol. 35, no. 3, pp. 473–485, May 2013, doi: 10.1016/j.etap.2013.02.011.

[41] A. P. Subramanian *et al.*, “Gallic Acid: Prospects and the molecular mechanisms of its anticancer activity.,” in *The Royal Society of Chemistry*, American Institute of Chemical Engineers, 2015. doi: 10.1039/x0xx00000x.

[42] A. De Cristo Soares Alves, R. M. Mainardes, and N. M. Khalil, “Nanoencapsulation of gallic acid and evaluation of its cytotoxicity and antioxidant activity,” *Materials Science and Engineering C*, vol. 60, pp. 126–134, Mar. 2016, doi: 10.1016/j.msec.2015.11.014.

[43] Z. Jing *et al.*, “Gallic acid-gold nanoparticles enhance radiation-induced cell death of human glioma U251 cells,” *IUBMB Life*, vol. 73, no. 2, pp. 398–407, Feb. 2021, doi: 10.1002/iub.2436.

[44] Y. Lu *et al.*, “Gallic acid suppresses cell viability, proliferation, invasion and angiogenesis in human glioma cells,” *Eur J Pharmacol*, vol. 641, no. 2–3, pp. 102–107, 2010, doi: 10.1016/j.ejphar.2010.05.043.

[45] D. J. Bharali *et al.*, “Nanoparticle delivery of natural products in the prevention and treatment of cancers: Current status and future prospects,” *Cancers*, vol. 3, no. 4. pp. 4024–4045, Dec. 2011. doi: 10.3390/cancers3044024.

[46] D. Furtado, M. Björnmalm, S. Ayton, A. I. Bush, K. Kempe, and F. Caruso, “Overcoming the Blood–Brain Barrier: The Role of Nanomaterials in Treating Neurological Diseases,” *Advanced Materials*, vol. 30, no. 46. Wiley-VCH Verlag, Nov. 15, 2018. doi: 10.1002/adma.201801362.

[47] M. Fakhoury, “Drug delivery approaches for the treatment of glioblastoma multiforme,” *Artificial Cells, Nanomedicine and Biotechnology*, vol. 44, no. 6. Taylor and Francis Ltd., pp. 1365–1373, Aug. 17, 2016. doi: 10.3109/21691401.2015.1052467.

[48] L. A. Bors and F. Erdö, “Overcoming the blood-brain barrier. Challenges and tricks for CNS drug delivery,” *Scientia Pharmaceutica*, vol. 87, no. 1. MDPI AG, Mar. 01, 2019. doi: 10.3390/scipharm87010006.

[49] O. Van Tellingen, B. Yetkin-Arik, M. C. De Gooijer, P. Wesseling, T. Wurdinger, and H. E. De Vries, “Overcoming the blood-brain tumor barrier for effective glioblastoma

treatment," *Drug Resistance Updates*, vol. 19. Churchill Livingstone, pp. 1–12, Mar. 01, 2015. doi: 10.1016/j.drup.2015.02.002.

[50] A. E. Caprifico, P. J. S. Foot, E. Polycarpou, and G. Calabrese, "Overcoming the blood-brain barrier: Functionalised chitosan nanocarriers," *Pharmaceutics*, vol. 12, no. 11, pp. 1–20, Nov. 2020, doi: 10.3390/pharmaceutics12111013.

[51] S. Bayda, M. Adeel, T. Tuccinardi, M. Cordani, and F. Rizzolio, "The history of nanoscience and nanotechnology: From chemical-physical applications to nanomedicine," *Molecules*, vol. 25, no. 1. MDPI AG, 2020. doi: 10.3390/molecules25010112.

[52] J. Silva, A. R. Fernandes, and P. V. Baptista, "Application of Nanotechnology in Drug Delivery," in *Application of Nanotechnology in Drug Delivery*, InTech, 2014. doi: 10.5772/58424.

[53] X. Xu, W. Ho, X. Zhang, N. Bertrand, and O. Farokhzad, "Cancer nanomedicine: From targeted delivery to combination therapy," *Trends in Molecular Medicine*, vol. 21, no. 4. Elsevier Ltd, pp. 223–232, Apr. 01, 2015. doi: 10.1016/j.molmed.2015.01.001.

[54] Y. Nakamura, A. Mochida, P. L. Choyke, and H. Kobayashi, "Nanodrug Delivery: Is the Enhanced Permeability and Retention Effect Sufficient for Curing Cancer?," *Bioconjugate Chemistry*, vol. 27, no. 10. American Chemical Society, pp. 2225–2238, Oct. 19, 2016. doi: 10.1021/acs.bioconjchem.6b00437.

[55] C. Zhan and W. Lu, "Send Orders of Reprints at reprints@benthamscience.org The Blood-Brain/Tumor Barriers: Challenges and Chances for Malignant Gliomas Targeted Drug Delivery," 2012.

[56] X. Xie *et al.*, "Challenges and Opportunities from Basic Cancer Biology for Nanomedicine for Targeted Drug Delivery," *Curr Cancer Drug Targets*, vol. 19, no. 4, pp. 257–276, Jun. 2018, doi: 10.2174/1568009618666180628160211.

[57] A. C. Anselmo and S. Mitragotri, "Nanoparticles in the clinic: An update," *Bioeng Transl Med*, vol. 4, no. 3, Sep. 2019, doi: 10.1002/btm2.10143.

[58] A. K. Biswas, M. R. Islam, Z. S. Choudhury, A. Mostafa, and M. F. Kadir, "Nanotechnology based approaches in cancer therapeutics," *Advances in Natural Sciences: Nanoscience and Nanotechnology*, vol. 5, no. 4, Dec. 2014, doi: 10.1088/2043-6262/5/4/043001.

[59] Y. Li *et al.*, "Betulinic acid self-assembled nanoparticles for effective treatment of glioblastoma," *J Nanobiotechnology*, vol. 20, no. 1, Dec. 2022, doi: 10.1186/s12951-022-01238-7.

[60] M. D. Mauricio *et al.*, "Nanoparticles in medicine: A focus on vascular oxidative stress," *Oxidative Medicine and Cellular Longevity*, vol. 2018. Hindawi Limited, 2018. doi: 10.1155/2018/6231482.

[61] A. A. H. Abdellatif and A. F. Alsowinea, “Approved and marketed nanoparticles for disease targeting and applications in COVID-19,” *Nanotechnology Reviews*, vol. 10, no. 1. De Gruyter Open Ltd, pp. 1941–1977, Jan. 01, 2021. doi: 10.1515/ntrev-2021-0115.

[62] D. S. Hersh *et al.*, “Send Orders for Reprints to reprints@benthamscience.ae Evolving Drug Delivery Strategies to Overcome the Blood Brain Barrier,” 2016.

[63] S. M. Curley and N. C. Cady, “Biologically-derived nanomaterials for targeted therapeutic delivery to the brain,” *Sci Prog*, vol. 101, no. 3, pp. 273–292, 2018, doi: 10.3184/003685018X15306123582346.

[64] P. I. Siafaka, N. Üstündağ Okur, E. Karavas, and D. N. Bikiaris, “Surface modified multifunctional and stimuli responsive nanoparticles for drug targeting: Current status and uses,” *International Journal of Molecular Sciences*, vol. 17, no. 9. MDPI AG, Sep. 01, 2016. doi: 10.3390/ijms17091440.

[65] M. J. Ramalho, M. Bravo, J. A. Loureiro, J. Lima, and M. C. Pereira, “Transferrin-modified nanoparticles for targeted delivery of Asiatic acid to glioblastoma cells,” *Life Sci*, vol. 296, May 2022, doi: 10.1016/j.lfs.2022.120435.

[66] M. Mahmoudi Saber, “Strategies for surface modification of gelatin-based nanoparticles,” *Colloids and Surfaces B: Biointerfaces*, vol. 183. Elsevier B.V., Nov. 01, 2019. doi: 10.1016/j.colsurfb.2019.110407.

[67] M. Shilo, M. Motiei, P. Hana, and R. Popovtzer, “Transport of nanoparticles through the blood-brain barrier for imaging and therapeutic applications,” *Nanoscale*, vol. 6, no. 4, pp. 2146–2152, Feb. 2014, doi: 10.1039/c3nr04878k.

[68] S. Beg *et al.*, “Novel surface-engineered solid lipid nanoparticles of rosuvastatin calcium for low-density lipoprotein-receptor targeting: A Quality by Design-driven perspective,” *Nanomedicine*, vol. 12, no. 4, pp. 333–356, Feb. 2017, doi: 10.2217/nnm-2016-0336.

[69] A. M. Gazzali *et al.*, “Stability of folic acid under several parameters,” *European Journal of Pharmaceutical Sciences*, vol. 93. Elsevier B.V., pp. 419–430, Oct. 10, 2016. doi: 10.1016/j.ejps.2016.08.045.

[70] M. Li *et al.*, “Synergistic tumor microenvironment targeting and blood–brain barrier penetration via a pH-responsive dual-ligand strategy for enhanced breast cancer and brain metastasis therapy,” *Nanomedicine*, vol. 14, no. 6, pp. 1833–1843, Aug. 2018, doi: 10.1016/j.nano.2018.05.008.

[71] S. Ding *et al.*, “Overcoming blood–brain barrier transport: Advances in nanoparticle-based drug delivery strategies,” *Materials Today*, vol. 37. Elsevier B.V., pp. 112–125, Jul. 01, 2020. doi: 10.1016/j.mattod.2020.02.001.

[72] M. J. Ramalho, M. Bravo, J. A. Loureiro, J. Lima, and M. C. Pereira, “Transferrin-modified nanoparticles for targeted delivery of Asiatic acid to glioblastoma cells,” *Life Sci*, vol. 296, May 2022, doi: 10.1016/j.lfs.2022.120435.

[73] H. Zhang *et al.*, “Development of curcumin-loaded zein nanoparticles for transport across the blood-brain barrier and inhibition of glioblastoma cell growth,” *Biomater Sci*, vol. 9, no. 21, pp. 7092–7103, Nov. 2021, doi: 10.1039/d0bm01536a.

[74] H. Nejat *et al.*, “Preparation and characterization of cardamom extract-loaded gelatin nanoparticles as effective targeted drug delivery system to treat glioblastoma,” *React Funct Polym*, vol. 120, pp. 46–56, Nov. 2017, doi: 10.1016/j.reactfunctpolym.2017.09.008.

[75] X. M. Lin *et al.*, “Construction of il-13 receptor α2-targeting resveratrol nanoparticles against glioblastoma cells: Therapeutic efficacy and molecular effects,” *Int J Mol Sci*, vol. 22, no. 19, Oct. 2021, doi: 10.3390/ijms221910622.

[76] K. T. Householder *et al.*, “Intravenous delivery of camptothecin-loaded PLGA nanoparticles for the treatment of intracranial glioma,” *Int J Pharm*, vol. 479, no. 2, pp. 374–380, Feb. 2015, doi: 10.1016/j.ijpharm.2015.01.002.

[77] M. Ersoz, A. Erdemir, S. Derman, T. Arasoglu, and B. Mansuroglu, “Quercetin-loaded nanoparticles enhance cytotoxicity and antioxidant activity on C6 glioma cells,” *Pharm Dev Technol*, vol. 25, no. 6, pp. 757–766, Jul. 2020, doi: 10.1080/10837450.2020.1740933.

[78] I. Meteoglu and A. Erdemir, “Genistein and Temozolomide-Loaded Polymeric Nanoparticles: A Synergistic Approach For Improved Anti-Tumor Efficacy Against Glioblastoma,” *Process Biochemistry*, vol. 110, pp. 9–18, Nov. 2021, doi: 10.1016/j.procbio.2021.07.015.

[79] E. R. de Oliveira Junior, T. L. Nascimento, M. A. Salomão, A. C. G. da Silva, M. C. Valadares, and E. M. Lima, “Increased Nose-to-Brain Delivery of Melatonin Mediated by Polycaprolactone Nanoparticles for the Treatment of Glioblastoma,” *Pharm Res*, vol. 36, no. 9, Sep. 2019, doi: 10.1007/s11095-019-2662-z.

[80] M. Colombo, F. Figueiró, A. de Fraga Dias, H. F. Teixeira, A. M. O. Battastini, and L. S. Koester, “Kaempferol-loaded mucoadhesive nanoemulsion for intranasal administration reduces glioma growth in vitro,” *Int J Pharm*, vol. 543, no. 1–2, pp. 214–223, May 2018, doi: 10.1016/j.ijpharm.2018.03.055.

[81] G. Deng *et al.*, “Anti-edema and antioxidant combination therapy for ischemic stroke via glyburide-loaded betulinic acid nanoparticles,” *Theranostics*, vol. 9, no. 23, pp. 6991–7002, 2019, doi: 10.7150/thno.35791.

[82] S. Paranthaman *et al.*, “Anti-Proliferative Potential of Quercetin Loaded Polymeric Mixed Micelles on Rat C6 and Human U87MG Glioma Cells,” *Pharmaceutics*, vol. 14, no. 8, Aug. 2022, doi: 10.3390/pharmaceutics14081643.

[83] D. Bartczak and A. G. Kanaras, “Preparation of peptide-functionalized gold nanoparticles using one pot EDC/Sulfo-NHS coupling,” *Langmuir*, vol. 27, no. 16, pp. 10119–10123, Aug. 2011, doi: 10.1021/la2022177.

[84] J. Gilman, L. Walls, L. Bandiera, and F. Menolascina, “Statistical Design of Experiments for Synthetic Biology,” *ACS Synthetic Biology*, vol. 10, no. 1. American Chemical Society, pp. 1–18, Jan. 15, 2021. doi: 10.1021/acssynbio.0c00385.

[85] J. Lamarra, S. Rivero, and A. Pinotti, “Design of chitosan-based nanoparticles functionalized with gallic acid,” *Materials Science and Engineering C*, vol. 67, pp. 717–726, Oct. 2016, doi: 10.1016/j.msec.2016.05.072.

[86] T. Rakić, I. Kasagić-Vujanović, M. Jovanović, B. Jančić-Stojanović, and D. Ivanović, “Comparison of Full Factorial Design, Central Composite Design, and Box-Behnken Design in Chromatographic Method Development for the Determination of Fluconazole and Its Impurities,” *Anal Lett*, vol. 47, no. 8, pp. 1334–1347, 2014, doi: 10.1080/00032719.2013.867503.

[87] S. Bhattacharya, “Central Composite Design for Response Surface Methodology and Its Application in Pharmacy,” 200AD. [Online]. Available: www.intechopen.com

[88] J. R. Wagner, E. M. Mount, and H. F. Giles, *Extrusion: The Definitive Processing Guide and Handbook: Second Edition*. Elsevier Inc., 2013. doi: 10.1016/C2010-0-67040-4.

[89] B. Ait-Amir, P. Pougnet, and A. El Hami, “Meta-Model Development,” *Embedded Mechatronic Systems 2: Analysis of Failures, Modeling, Simulation and Optimization*, pp. 157–187, Jan. 2020, doi: 10.1016/B978-1-78548-190-1.50006-2.

[90] J. Stetefeld, S. A. McKenna, and T. R. Patel, “Dynamic light scattering: a practical guide and applications in biomedical sciences,” *Biophysical Reviews*, vol. 8, no. 4. Springer Verlag, pp. 409–427, Dec. 01, 2016. doi: 10.1007/s12551-016-0218-6.

[91] “Malvern Panalytical | Analytical Instrumentation.” https://www.malvernpanalytical.com/br?campaignid=125191521&adgroupid=7526818161&creative=319484801988&keyword=malvern%20panalytical&matchtype=p&network=g&device=c&pk_campaign=125191521&pk_adgroupid=7526818161&pk_kwd=malvern%20panalytical&pk_source=google&pk_medium=cpc&pk_content=319484801988&gclid=CjwKCAiA2rOeBhAsEiwA2Pl7QwSbS8TZ2uWYMHg8CCXg7tLCaISsvrd2kkouGlFoGX23Qk1iPx-EBhoCB9AQAvD_BwE (accessed Jan. 23, 2023).

[92] S. Bhattacharjee, “DLS and zeta potential - What they are and what they are not?,” *Journal of Controlled Release*, vol. 235. Elsevier B.V., pp. 337–351, Aug. 10, 2016. doi: 10.1016/j.jconrel.2016.06.017.

[93] P. M. Carvalho, M. R. Felício, N. C. Santos, S. Gonçalves, and M. M. Domingues, “Application of light scattering techniques to nanoparticle characterization and development,” *Frontiers in Chemistry*, vol. 6. Frontiers Media S.A., Jun. 01, 2018. doi: 10.3389/fchem.2018.00237.

[94] “Dynamic Light Scattering: DLS Particle Analyzer :: Microtrac.” https://www.microtrac.com/products/particle-size-shape-analysis/dynamic-light-scattering-zeta-potential/?gclid=CjwKCAiA2rOeBhAsEiwA2Pl7QwZHE5dV2T1OM7vkSR154s413KSG66C5XgwX_oWXpktTFIn9-ckUlRoCZ44QAvD_BwE (accessed Jan. 23, 2023).

[95] E. Piacentini, *Encapsulation Efficiency*. Springer, Berlin, Heidelberg, 2016. doi: 10.1007/978-3-662-44324-8_1945.

[96] B. Ladewig and M. N. Z. Al-Shaeli, “Membrane Characterization Techniques,” 2017, pp. 131–150. doi: 10.1007/978-981-10-2014-8_5.

[97] M. A. Mohamed, J. Jaafar, A. F. Ismail, M. H. D. Othman, and M. A. Rahman, “Fourier Transform Infrared (FTIR) Spectroscopy,” in *Membrane Characterization*, Elsevier Inc., 2017, pp. 3–29. doi: 10.1016/B978-0-444-63776-5.00001-2.

[98] M. Malatesta, “Transmission electron microscopy as a powerful tool to investigate the interaction of nanoparticles with subcellular structures,” *International Journal of Molecular Sciences*, vol. 22, no. 23. MDPI, Dec. 01, 2021. doi: 10.3390/ijms222312789.

[99] S. R. L, “Modification of the Uranyl Acetate Replacement Staining Protocol for Transmission Electron Microscopy,” *Int J Med Nano Res*, vol. 3, no. 1, Dec. 2016, doi: 10.23937/2378-3664/1410013.

[100] M. W. Tuijtel *et al.*, “Inducing fluorescence of uranyl acetate as a dual-purpose contrast agent for correlative light-electron microscopy with nanometre precision,” *Scientific Reports 2017 7:1*, vol. 7, no. 1, pp. 1–12, Sep. 2017, doi: 10.1038/s41598-017-10905-x.

[101] “PBS (Phosphate Buffered Saline) (1X, pH 7.4) Preparation and Recipe | AAT Bioquest.” https://www.aatbio.com/resources/buffer-preparations-and-recipes/pbs-phosphate-buffered-saline (accessed May 31, 2023).

[102] J. J. Walsh *et al.*, “Imaging Hallmarks of the Tumor Microenvironment in Glioblastoma Progression,” *Front Oncol*, vol. 11, p. 3307, Aug. 2021, doi: 10.3389/FONC.2021.692650/BIBTEX.

[103] E. Proksch, “pH in nature, humans and skin,” *Journal of Dermatology*, vol. 45, no. 9. Blackwell Publishing Ltd, pp. 1044–1052, Sep. 01, 2018. doi: 10.1111/1346-8138.14489.

[104] M. S. Shakil, Z. Rana, M. Hanif, and R. J. Rosengren, “Key considerations when using the sulforhodamine B assay for screening novel anticancer agents,” *Anticancer Drugs*, vol. 33, no. 1, pp. 6–10, Jan. 2022, doi: 10.1097/CAD.0000000000001131.

[105] W. Huang and C. Zhang, “Tuning the size of poly(lactic-co-glycolic acid) (PLGA) nanoparticles fabricated by nanoprecipitation; Tuning the size of poly(lactic-co-glycolic acid) (PLGA) nanoparticles fabricated by nanoprecipitation”, doi: 10.1002/biot.201600203.

[106] Y. Liu, J. Pan, and S. S. Feng, “Nanoparticles of lipid monolayer shell and biodegradable polymer core for controlled release of paclitaxel: Effects of surfactants on particles size, characteristics and in vitro performance,” *Int J Pharm*, vol. 395, no. 1–2, pp. 243–250, Aug. 2010, doi: 10.1016/J.IJPHARM.2010.05.008.

[107] X. ting CHEN and T. Wang, “Preparation and characterization of atrazine-loaded biodegradable PLGA nanospheres,” *J Integr Agric*, vol. 18, no. 5, pp. 1035–1041, May 2019, doi: 10.1016/S2095-3119(19)62613-4.

[108] L. R. Tefas, I. Tomuță, M. Achim, and L. Vlase, “Development and optimization of quercetin-loaded plga nanoparticles by experimental design,” *Clujul Medical*, vol. 88, no. 2, pp. 214–223, 2015, doi: 10.15386/cjmed-418.

[109] M. Wiśniewska *et al.*, “Investigation of the polyvinyl alcohol stabilization mechanism and adsorption properties on the surface of ternary mixed nanooxide AST 50 (Al2O3–SiO2–TiO2),” *Journal of Nanoparticle Research*, vol. 17, no. 1, Jan. 2015, doi: 10.1007/s11051-014-2831-2.

[110] E. Ruiz, V. H. Orozco, L. M. Hoyos, and L. F. Giraldo, “Study of sonication parameters on PLA nanoparticles preparation by simple emulsion-evaporation solvent technique,” *Eur Polym J*, vol. 173, Jun. 2022, doi: 10.1016/j.eurpolymj.2022.111307.

[111] S. Mura *et al.*, “Influence of surface charge on the potential toxicity of PLGA nanoparticles towards Calu-3 cells.,” *Int J Nanomedicine*, vol. 6, pp. 2591–2605, 2011, doi: 10.2147/ijn.s24552.

[112] M. V. Shaikh, M. Kala, and M. Nivsarkar, “Formulation and optimization of doxorubicin loaded polymeric nanoparticles using Box-Behnken design: ex-vivo stability and in-vitro activity,” *European Journal of Pharmaceutical Sciences*, vol. 100, pp. 262–272, Mar. 2017, doi: 10.1016/j.ejps.2017.01.026.

[113] R. Saadati and S. Dadashzadeh, “Marked effects of combined TPGS and PVA emulsifiers in the fabrication of etoposide-loaded PLGA-PEG nanoparticles: In vitro and in vivo evaluation,” *Int J Pharm*, vol. 464, no. 1–2, pp. 135–144, Apr. 2014, doi: 10.1016/j.ijpharm.2014.01.014.

[114] Q. T. H. Shubhra *et al.*, “Co-encapsulation of human serum albumin and superparamagnetic iron oxide in PLGA nanoparticles: Part II. Effect of process variables on protein model drug encapsulation efficiency,” *J Microencapsul*, vol. 31, no. 2, pp. 156–165, 2014, doi: 10.3109/02652048.2013.814730.

[115] S. Taymouri, J. Varshosaz, S. Taymouri, H. Hamishehkar, R. Vatankhah, and S. Yaghubi, “Development of dry powder inhaler containing tadalafil-loaded PLGA nanoparticles,” *Res Pharm Sci*, vol. 12, no. 3, pp. 222–232, Jun. 2017, doi: 10.4103/1735-5362.207203.

[116] C. Berthomieu and R. Hienerwadel, “Fourier transform infrared (FTIR) spectroscopy,” *Photosynthesis Research*, vol. 101, no. 2–3. pp. 157–170, Sep. 2009. doi: 10.1007/s11120-009-9439-x.

[117] G. Singh, A. Kaur, T. Kaur, and R. Kaur, “Recent biomedical applications and patents on biodegradable polymer-PLGA,” 2014. [Online]. Available: http://ijppsjournal.org

[118] K. Essifi, M. Lakrat, D. Berraaouan, M. L. Fauconnier, A. El Bachiri, and A. Tahani, “Optimization of gallic acid encapsulation in calcium alginate microbeads using Box-Behnken Experimental Design,” *Polymer Bulletin*, vol. 78, no. 10, pp. 5789–5814, Oct. 2021, doi: 10.1007/s00289-020-03397-9.

[119] S. Rana, N. G. Shetake, K. C. Barick, B. N. Pandey, H. G. Salunke, and P. A. Hassan, “Electronic Supplementary Information (ESI) Folic acid Conjugated Fe 3 O 4 Magnetic Nanoparticles for Targeted Delivery of Doxorubicin,” *Dalton Transactions*, vol. 45, no. 43, Sep. 2016, doi: 10.1039/C6DT03323G.

[120] Y. Y. He, X. C. Wang, P. K. Jin, B. Zhao, and X. Fan, “Complexation of anthracene with folic acid studied by FTIR and UV spectroscopies,” *Spectrochim Acta A Mol Biomol Spectrosc*, vol. 72, no. 4, pp. 876–879, May 2009, doi: 10.1016/j.saa.2008.12.021.

[121] K. Nagpal, S. K. Singh, and D. N. Mishra, “Optimization of brain targeted gallic acid nanoparticles for improved antianxiety-like activity,” *Int J Biol Macromol*, vol. 57, pp. 83–91, 2013, doi: 10.1016/j.ijbiomac.2013.03.022.

[122] J. Weng, H. H. Y. Tong, and S. F. Chow, “In vitro release study of the polymeric drug nanoparticles: Development and validation of a novel method,” *Pharmaceutics*, vol. 12, no. 8, pp. 1–18, Aug. 2020, doi: 10.3390/pharmaceutics12080732.

[123] I. Negut, V. Grumezescu, and G. Dorcioman, “Chapter 6- Progress of nanoparticles research in cancer therapy and diagnosis,” in *Nanostructures for Cancer Therapy*, Anton Ficai and Alexandru Mihai Grumezescu, Eds., Elsevier, 2017, pp. 159–176.

[124] B. Lu, X. Lv, and Y. Le, “Chitosan-modified PLGA nanoparticles for control-released drug delivery,” *Polymers (Basel)*, vol. 11, no. 2, Feb. 2019, doi: 10.3390/polym11020304.

[125] D. J. Hines and D. L. Kaplan, “Poly (lactic-co-glycolic acid) controlled release systems: experimental and modeling insights,” *Critical reviews in therapeutic drug carrier systems*, vol. 30, no. 3, pp. 257–276, 2013.

[126] R. Roberts *et al.*, “Development of PLGA nanoparticles for sustained release of a connexin43 mimetic peptide to target glioblastoma cells,” *Materials Science and Engineering C*, vol. 108, Mar. 2020, doi: 10.1016/j.msec.2019.110191.

[127] G. Midekessa *et al.*, “Zeta Potential of Extracellular Vesicles: Toward Understanding the Attributes that Determine Colloidal Stability,” *ACS Omega*, vol. 5, no. 27, pp. 16701–16710, Jul. 2020, doi: 10.1021/acsomega.0c01582.

[128] P. Bihari *et al.*, “Optimized dispersion of nanoparticles for biological in vitro and in vivo studies,” *Part Fibre Toxicol*, vol. 5, Nov. 2008, doi: 10.1186/1743-8977-5-14.

[129] X. Li *et al.*, “Ex-Situ Synthesis of Polyvinyl alcohol(PVA)-coated Fe 3 O 4 Nanoparticles by Coprecipitation-Ultrasonication Method You may also like Optimization of entrapping conditions to improve the release of BMP-2 from PELA carriers by response surface

methodology Hydrothermal synthesis of BaTiO 3 nanoparticles and role of PVA concentration in preparation Ex-Situ Synthesis of Polyvinyl alcohol(PVA)-coated Fe 3 O 4 Nanoparticles by Coprecipitation-Ultrasonication Method," *IOP Conf Ser Mater Sci Eng*, vol. 299, no. 1, Jan. 2018, doi: 10.1088/1757-899X/299/1/012065.

[130] S. Aykul and E. Martinez-Hackert, "Determination of half-maximal inhibitory concentration using biosensor-based protein interaction analysis," *Anal Biochem*, vol. 508, pp. 97–103, Sep. 2016, doi: 10.1016/j.ab.2016.06.025.

[131] S. S. Hsu *et al.*, "The effect of gallic acid on cytotoxicity, Ca2+ homeostasis and ROS production in DBTRG-05MG human glioblastoma cells and CTX TNA2 rat astrocytes," *Chem Biol Interact*, vol. 252, pp. 61–73, May 2016, doi: 10.1016/j.cbi.2016.04.010.

Appendix

A1. Calibration Curve

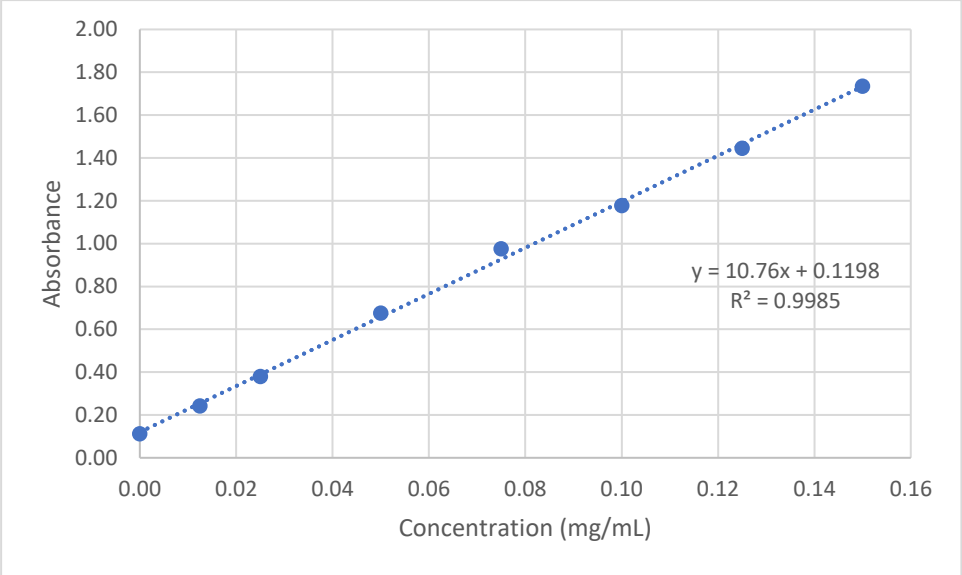


Figure A1. 1- Absorbance calibration curve of GA in PVA 1% to determine the EE of GA.

A2. Experimental Design

Table A2. 1 - ANOVA analysis for the response variable Size (Y_1) applying a quartic model.

Size (Y_1)						
Source	Sum of Squares	df	Mean Square	F-value	p-value	
Model	56949,58	24	2372,90	34,99	0,0004	significant
A-PLGA	435,13	1	435,13	6,42	0,0523	
B-PVA	26865,62	1	26865,62	396,14	< 0.0001	
C-FA	14,58	1	14,58	0,2150	0,6624	
D-Sonication	406,13	1	406,13	5,99	0,0581	
AB	842,45	1	842,45	12,42	0,0168	
AC	133,98	1	133,98	1,98	0,2188	
AD	28,89	1	28,89	0,4260	0,5428	
BC	1077,48	1	1077,48	15,89	0,0105	
BD	956,36	1	956,36	14,10	0,0132	
CD	95,55	1	95,55	1,41	0,2886	
A^2	1085,42	1	1085,42	16,00	0,0103	
B^2	16364,70	1	16364,70	241,30	< 0.0001	
C^2	120,15	1	120,15	1,77	0,2406	
D^2	50,46	1	50,46	0,7440	0,4278	
ABC	40,64	1	40,64	0,5993	0,4739	
ABD	52,93	1	52,93	0,7804	0,4175	
ACD	144,60	1	144,60	2,13	0,2041	
BCD	22,33	1	22,33	0,3292	0,5910	
A^2B	13337,89	1	13337,89	196,67	< 0.0001	
A^2C	2,30	1	2,30	0,0338	0,8613	
A^2D	0,2177	1	0,2177	0,0032	0,9570	
AB^2	1043,28	1	1043,28	15,38	0,0112	
ABCD	7,43	1	7,43	0,1095	0,7541	
A^2B^2	4767,22	1	4767,22	70,29	0,0004	
Pure Error	339,09	5	67,82			
Cor Total	57288,68	29				

Table A2. 2 - ANOVA analysis for the response variable PDI (Y_2) applying a quartic model.

PDI (Y_2)						
Source	Sum of Squares	df	Mean Square	F-value	p-value	
Model	0,0890	24	0,0037	31,76	0,0006	significant
A-PLGA	0,0300	1	0,0300	256,96	< 0.0001	
B-PVA	0,0001	1	0,0001	1,24	0,3166	
C-FA	5,000E-07	1	5,000E-07	0,0043	0,9504	
D-Sonication	0,0011	1	0,0011	9,46	0,0276	
AB	0,0010	1	0,0010	8,63	0,0323	
AC	0,0008	1	0,0008	6,59	0,0502	
AD	0,0000	1	0,0000	0,3344	0,5881	
BC	0,0005	1	0,0005	3,87	0,1064	
BD	0,0002	1	0,0002	2,12	0,2048	
CD	7,563E-06	1	7,563E-06	0,0647	0,8093	
A^2	0,0416	1	0,0416	356,02	< 0.0001	
B^2	0,0059	1	0,0059	50,17	0,0009	
C^2	0,0003	1	0,0003	2,34	0,1866	
D^2	0,0001	1	0,0001	0,7224	0,4342	
ABC	1,562E-06	1	1,562E-06	0,0134	0,9124	
ABD	0,0005	1	0,0005	4,43	0,0892	
ACD	0,0008	1	0,0008	6,59	0,0502	
BCD	0,0003	1	0,0003	2,85	0,1521	
A^2B	0,0000	1	0,0000	0,1336	0,7297	
A^2C	0,0003	1	0,0003	2,91	0,1485	
A^2D	0,0003	1	0,0003	2,22	0,1968	
AB^2	0,0202	1	0,0202	172,74	< 0.0001	
ABCD	0,0002	1	0,0002	1,50	0,2748	
A^2B^2	0,0180	1	0,0180	154,24	< 0.0001	
Pure Error	0,0006	5	0,0001			
Cor Total	0,0896	29				

Table A2. 3 - ANOVA analysis for the response variable Zeta Potential (Y_3) applying a quartic model.

Zeta (Y_3)						
Source	Sum of Squares	df	Mean Square	F-value	p-value	
Model	638,18	24	26,59	11,42	0,0065	significant
A-PLGA	1,62	1	1,62	0,6955	0,4423	
B-PVA	9,95	1	9,95	4,27	0,0937	
C-FA	1,08	1	1,08	0,4639	0,5261	
D-Sonication	4,12	1	4,12	1,77	0,2410	
AB	6,88	1	6,88	2,95	0,1464	
AC	13,52	1	13,52	5,81	0,0609	
AD	0,0977	1	0,0977	0,0419	0,8458	
BC	117,34	1	117,34	50,38	0,0009	
BD	5,65	1	5,65	2,43	0,1800	
CD	1,02	1	1,02	0,4358	0,5383	
A^2	0,8702	1	0,8702	0,3736	0,5678	
B^2	3,66	1	3,66	1,57	0,2655	
C^2	1,90	1	1,90	0,8175	0,4074	
D^2	1,58	1	1,58	0,6788	0,4475	
ABC	2,90	1	2,90	1,24	0,3153	
ABD	0,0086	1	0,0086	0,0037	0,9540	
ACD	0,0001	1	0,0001	0,0000	0,9963	
BCD	0,8327	1	0,8327	0,3575	0,5759	
A^2B	76,29	1	76,29	32,75	0,0023	
A^2C	14,34	1	14,34	6,16	0,0557	
A^2D	0,0853	1	0,0853	0,0366	0,8558	
AB^2	14,11	1	14,11	6,06	0,0571	
ABCD	5,63	1	5,63	2,42	0,1808	
A^2B^2	70,21	1	70,21	30,15	0,0027	
Pure Error	11,65	5	2,33			
Cor Total	649,83	29				

Table A2. 4 - ANOVA analysis for the response variable GA EE (Y_4) applying a linear model.

GA EE (Y_4)						
Source	Sum of Squares	df	Mean Square	F-value	p-value	
Model	3824.88	4	956.22	11.17	<0.0001	significant
A-PLGA Mass	42.88	1	42.88	0.5008	0.4857	
B-%PVA	3739.55	1	3739.55	43.68	<0.0001	
C-Fa molecules/NP	17.40	1	17.40	0.2032	0.6560	
D-Sonication Cycles	25.06	1	25.06	0.2927	0.5933	
Residual	2140.25	25	85.61			
Lack of Fit	1722.24	20	86.11	1.03	0.5409	not significant
Pure Error	418.01	5	83.60			
Cor Total	5965.14	29				

A2.1 NPs Size

Size = 151.45 -9.54 (PLGA mass) – 74.93 * (%PVA) – 1.75 (FA molecules/NP) - 9.21 (Sonication Cycles) – 7.26 (PLGA mass) (%PVA) (1)

- 8.21 (%PVA) (FA molecules/NP) - 7.73 (%PVA) (Sonication Cycles) + 11.24 (PLGA mass)^2 + 43.66 (%PVA)^2 + 60.18 (PLGA mass)^2 (%PVA) + 16.83 (PLGA mass) (%PVA)^2 - 48.19 (PLGA mass)^2 (%PVA)^2

A2.2 NPs PDI

PDI = 0.0440 – 0.0792 (PLGA mass) – 0.0055 (%PVA) (2)

+ 0.0003 (FA molecules/NP) + 0.0152 (Sonication Cycles) – 0.0079 (PLGA mass) (%PVA) + 0.0696 (PLGA mass)^2 + 0.0261 (%PVA) + 0.0740 (PLGA mass) (%PVA)^2

$$- 0.0937 (\text{PLGA mass})^2 (\%\text{PVA})^2$$

A2.3 NPs Zeta Potential

$$\begin{aligned}\text{Zeta Potential} = {} & -19.54 - 0.5819 (\text{PLGA mass}) + 1.44 (\%\text{PVA}) \\ & + 0.4752 (\text{FA molecules/NP}) + 0.9278 (\text{Sonication Cycles}) \\ & - 7.26 (\%\text{PVA}) (\text{FA molecules/NP}) \\ & - 8.21 (\text{PLGA mass})^2 (\%\text{PVA}) - 7.73 (\text{PLGA mass})^2 (\%\text{PVA})^2\end{aligned} \quad (3)$$

A2.4 NPs EE

$$\begin{aligned}\text{GA EE} = {} & 40.91 + 1.44 (\text{PLGA mass}) + 13.41 (\%\text{PVA}) \\ & + 0.9149 (\text{FA molecules/NP}) + 1.10 (\text{Sonication Cycles})\end{aligned} \quad (4)$$

A3. GA Solubility and Stability Studies

Solubility studies of GA were performed for ethyal acetate (EA) and dimethyl sulfoxide (DMSO), and the solubility limit tested was 2 mg/mL. The prepared solution containing each organic solvent was subjected to mechanical agitation using a vortex (Heidolph Reax Top Vortex Mixer, Heidolph instruments GmbH & Co., Schwabach, Germany) for 5 min, and at the end of this period, the drug appeared visually diluted. To confirm it, the UV-vis absorbance spectra between 200-700 nm of the sample was measured using a microplate reader (Synergy 2 Microplate Reader, BioTek, UK). Both steps were performed cyclically until constant absorbance values were obtained between two consecutive measurements. The obtained results are presented in figures A3.1 and A3.2.

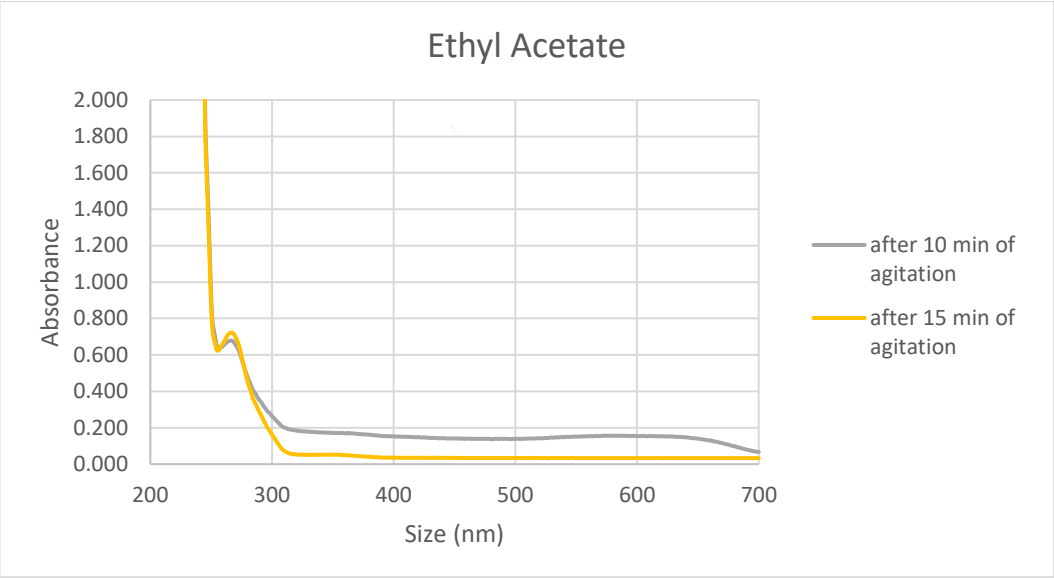


Figure A3. 1- Solubility of GA in ethyl acetate.

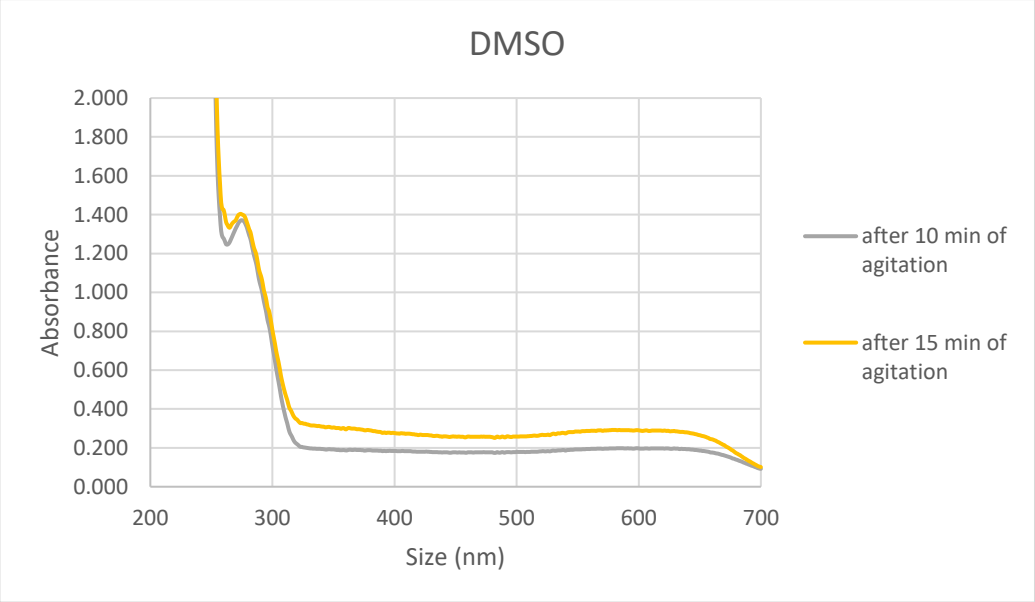


Figure A3. 2- Solubility of GA in DMSO.

For both organic solvents, it was necessary to submit the solution to three 5 min cycles of mechanical agitation to maintain the absorbance value. GA in EA showed the following absorbance values for the maximum absorbance wavelength (265 nm): 0.677 after 10 min of agitation, and 0.719 after 15 min of agitation. Thus, it was possible to conclude that the absorbance value didn't change significantly. For GA in DMSO, the absorbance values were recorded for the peak at 274 nm, obtaining: 1.37, and 1.40 in the two consecutive measurements. As the peak absorbance results didn´t change significantly, this suggests that GA was completely soluble in the organic solvent.

Since GA was soluble in both studied organic solvents after 15 min of agitation, both could be used for NPs preparation. EA was chosen since is the most suitable for a single-emulsion evaporation method. PLGA NPs can be prepared by a single-emulsion or double emulsion-

evaporation method depending on the hydrophobicity of the compound to encapsulate [80]. As GA is a hydrophobic molecule, EA was chosen for the procedure of single-emulsion. Thus, the GA stability in EA under the experimental conditions of NPs preparation was studied.

The conditions were mechanical agitation by vortex for 30 sec, followed by 2 rounds of 3 sonication cycles of 10-sec on/off with an amplitude of 70% and a frequency of 24 kHz (probe sonicator, UP400S, Hielscher, Berlin, Germany). The absorbance of the sample was measured before and after the stability tests and Figure A3.3, shown below, represents the absorbance presents the obtained results.

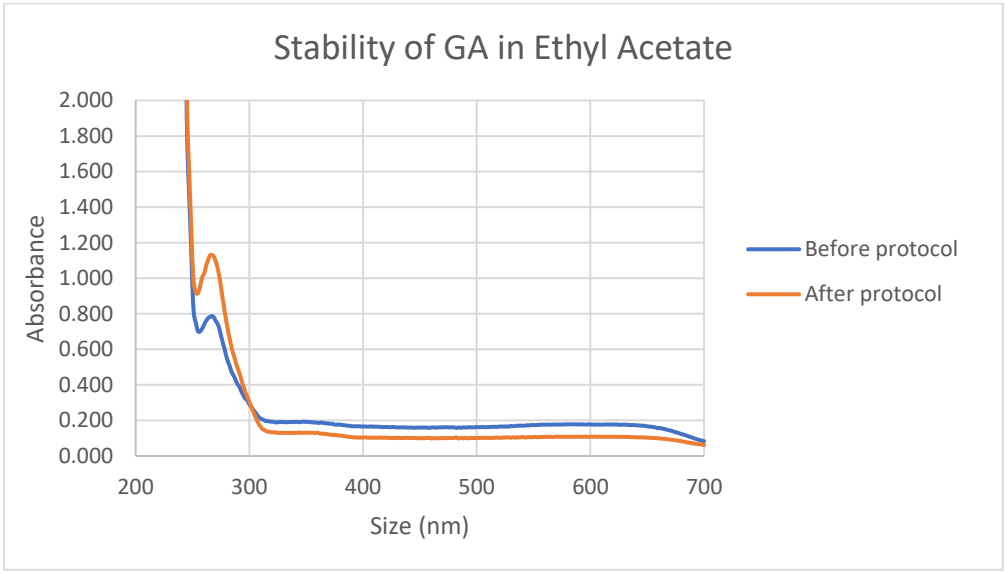


Figure A3. 3- Stability of GA in ethyl acetate.

The results show that the absorbance obtained between the measurements of the organic solution was different. This may be because EA is a solvent that evaporates very easily, and by performing the sonication of the solution, part of the solvent may have evaporated. Thus, the sample may have become more concentrated and hence there was an increase in the absorbance of the solution. Despite this result, ethyl acetate was used as the organic solvent in the NPs production protocol since the literature confirms the stability of GA in this solvent.